

1 **Chemical characterization of fine particulate matter in Changzhou, China**  
2 **and source apportionment with offline aerosol mass spectrometry**

3  
4 Zhaolian Ye<sup>1,2</sup>, Jiashu Liu<sup>1</sup>, Aijun Gu<sup>1</sup>, Feifei Feng<sup>1</sup>, Yuhai Liu<sup>1</sup>, Chenglu Bi<sup>1</sup>, Jianzhong  
5 Xu<sup>3</sup>, Ling Li<sup>2</sup>, Hui Chen<sup>2</sup>, Yanfang Chen<sup>2</sup>, Liang Dai<sup>2</sup>, Quanfa Zhou<sup>1</sup>, Xinlei Ge<sup>2,\*</sup>

6  
7 <sup>1</sup>College of Chemistry and Environmental Engineering, Jiangsu University of  
8 Technology, Changzhou 213001, China

9 <sup>2</sup>Jiangsu Key Laboratory of Atmospheric Environment Monitoring and Pollution  
10 Control, Collaborative Innovation Center of Atmospheric Environment and Equipment  
11 Technology, School of Environmental Sciences and Engineering, Nanjing University of  
12 Information Science and Technology, Nanjing 210044, China

13 <sup>3</sup>State Key Laboratory of Cryospheric Sciences, Northwest Institute of Eco-Environment  
14 and Resources, Chinese Academy of Sciences, Lanzhou 730000, China

15 \*Corresponding author, Email: [caxinra@163.com](mailto:caxinra@163.com)

16 Phone: +86-25-58731394

17  
18 **Abstract:** Knowledge on aerosol chemistry in densely populated regions is critical for  
19 effective reduction of air pollution, while such studies have not been conducted in  
20 Changzhou, an important manufacturing base and populated city in the Yangtze River  
21 Delta (YRD), China. This work, for the first time, performed a thorough chemical  
22 characterization on the fine particulate matter (PM<sub>2.5</sub>) samples, collected during July  
23 2015 to April 2016 across four seasons in this city. A suite of analytical techniques were  
24 employed to measure the organic carbon (OC), elemental carbon (EC), water-soluble  
25 organic carbon (WSOC), water-soluble inorganic ions (WSIIs), trace elements, and  
26 polycyclic aromatic hydrocarbons (PAHs) in PM<sub>2.5</sub>; in particular, an Aerodyne soot  
27 particle aerosol mass spectrometer (SP-AMS) was deployed to probe the chemical  
28 properties of water-soluble organic aerosols (WSOA). The average PM<sub>2.5</sub> concentrations  
29 were found to be 108.3 μg m<sup>-3</sup>, and all identified species were able to reconstruct ~80%  
30 of the PM<sub>2.5</sub> mass. The WSIIs occupied about half of the PM<sub>2.5</sub> mass (~52.1%), with

31  $\text{SO}_4^{2-}$ ,  $\text{NO}_3^-$  and  $\text{NH}_4^+$  as the major ions. On average, nitrate concentrations dominated  
32 over sulfate (mass ratio of 1.21), indicating that traffic emissions were more important  
33 than stationary sources. OC and EC correlated well with each other and the highest  
34 OC/EC ratio (5.16) occurred in winter, suggesting complex OC sources likely including  
35 both secondary and primary ones. Concentrations of eight trace elements (Mn, Zn, Al, B,  
36 Cr, Cu, Fe, Pb) can contribute up to  $\sim 5.0\%$  of  $\text{PM}_{2.5}$  during winter. PAHs concentrations  
37 were also high in winter ( $140.25 \text{ ng m}^{-3}$ ), which were predominated by median/high  
38 molecular weight PAHs with 5- and 6-rings. The organic matter including both  
39 water-soluble and water-insoluble species occupied  $\sim 21.5\%$   $\text{PM}_{2.5}$  mass. SP-AMS  
40 determined that the WSOA had an average atomic oxygen-to-carbon (O/C),  
41 hydrogen-to-carbon (H/C), nitrogen-to-carbon (N/C) and organic matter-to-organic  
42 carbon (OM/OC) ratios of 0.54, 1.69, 0.11, and 1.99, respectively. Source apportionment  
43 of WSOA further identified two secondary OA (SOA) factors (a less oxidized and a  
44 more oxidized oxygenated OA) and two primary OA (POA) factors (a nitrogen enriched  
45 hydrocarbon-like traffic OA and a local primary OA likely including species from  
46 cooking, coal combustion, etc.). On average, the POA contribution outweighed SOA  
47 (55% vs. 45%), indicating the important role of local anthropogenic emissions to the  
48 aerosol pollution in Changzhou. Our measurement also shows the abundance of organic  
49 nitrogen species in WSOA, and the source analyses suggest these species likely  
50 associated with traffic emissions, which warrants more investigations on PM samples  
51 from other locations.

52

## 53 **1. Introduction**

54 Aerosol particles are ubiquitous in the atmosphere and play important roles in air  
55 quality, global climate, biogeochemical cycle, and human health, etc (e.g., Heal et al.,  
56 2012;Cao et al., 2012;Hu et al., 2015). Aerosol pollution can also influence remote  
57 territories via long-range transport. Therefore, atmospheric aerosol has received  
58 extensive attentions from the government, public and academia (e.g., Zhang et al.,  
59 2007a;Jimenez et al., 2009). Particularly, much attentions have been focused on fine

60 particles (PM<sub>2.5</sub>, aerodynamic diameters less than 2.5 μm) as they can go deeper into the  
61 respiratory system, causing more severe health problems than coarse particles (Anderson  
62 et al., 2012). However, the concentrations, sources, chemical compositions and  
63 formation mechanisms of PM<sub>2.5</sub> are complicated and can vary greatly with  
64 meteorological conditions, seasons and regional/local topography, etc. PM<sub>2.5</sub> can contain  
65 a variety of species, i.e., organic carbon (OC), elemental carbon (EC), trace elements,  
66 inorganic salts, and various organic species such as polycyclic aromatic hydrocarbons  
67 (PAHs)(e.g., Wang et al., 2015). In China, haze pollution occurred frequently in recent  
68 years, and a large number of studies regarding the chemical characterization of fine  
69 particles were carried out in many locations (Wang et al., 2006a), such as Shanghai (e.g.,  
70 Wang et al., 2016a;Zhao et al., 2015), Beijing (e.g., Sun et al., 2014;Hu et al., 2016;Sun  
71 et al., 2016), Nanjing (e.g., Zhang et al., 2016;Ding et al., 2013), Lanzhou (e.g., Fan et  
72 al., 2014;Xu et al., 2014), Wuhan (e.g., Huang et al., 2016), and other remote sites (Xu  
73 et al., 2015), etc.

74 Yangtze River Delta (YRD) region, located in Eastern China, is experiencing  
75 severe atmospheric pollution along with the rapid economic development. Some studies  
76 carried out in the YRD investigated different characteristics of the fine aerosols,  
77 including the mass loading, composition, hygroscopicity (e.g., Ye et al., 2011;Ge et al.,  
78 2015), size distribution, seasonal variation, source, formation pathway, and their impacts  
79 on visibility and climate (e.g., Wang et al., 2012). However, these studies were mostly  
80 limited in Nanjing (e.g., Hu et al., 2012;Wang et al., 2016b) and Shanghai (e.g., Fu et al.,  
81 2012;Qiao et al., 2015;Wang et al., 2012). Changzhou, situated in the western YRD  
82 region, between Shanghai and Nanjing, is also a major city and an important  
83 manufacturing base due to its geographical advantage. The city has an area of about  
84 4374 km<sup>2</sup> with a population of 4.45 million. Due to elevated emissions of various  
85 pollutants, the number of hazy days increased over the past few years in Changzhou as  
86 well. To the best of our knowledge, no work has been published specifically on chemical  
87 characteristics and source apportionment of fine particles in Changzhou. Thus, it is  
88 scientifically and practically important to investigate the PM<sub>2.5</sub> characteristics in order to

89 provide efficient control strategies to reduce the PM pollution for Changzhou.

90 Among various PM<sub>2.5</sub> constituents, organic aerosol (OA) is a vital component,  
91 accounting for a significant, even dominant fraction of PM<sub>2.5</sub> in ambient air (Zhang et al.,  
92 2007a). Thus elucidation of its composition, properties and sources is essential.  
93 Apportionment of OA into different sources correctly is a critical step towards enabling  
94 efficient air pollution control strategies. Recently, Aerodyne Aerosol Mass spectrometry  
95 (AMS) has been used extensively for quantitatively characterizing ambient OA, and the  
96 \wealthy mass spectral data allows a better source analyses of OA (Canagaratna et al.,  
97 2007). Particularly, positive matrix factorization (PMF), as a standard multivariate factor  
98 analysis method, has been widely applied on AMS datasets to distinguish and quantify  
99 the OA sources (Zhang et al., 2011). Many previous studies (e.g., Ge et al., 2012a;Ng et  
100 al., 2011) have deployed the AMS for online field measurements since AMS can  
101 provide real-time information on mass concentrations and size distributions of aerosol  
102 particles with very fine time resolution (several seconds to minutes). However, up to  
103 now, AMS was typically used for online measurements and only a few studies made  
104 efforts to apply it on offline filter sample analyses and source apportionment (Ge et al.,  
105 2014;Daellenbach et al., 2016;Sun et al., 2011a;Bozzetti et al., 2017;Mihara and  
106 Mochida, 2011;Huang et al., 2014;Xu et al., 2015).

107 In this study, for the first time, we systematically investigated the chemical  
108 characteristics of ambient PM<sub>2.5</sub> collected in Changzhou nearly across one-year period,  
109 providing an overview about the concentrations of PM<sub>2.5</sub>, water-soluble inorganic ions  
110 (WSIIs), trace elements, carbonaceous species, water-soluble organic carbon (WSOC),  
111 and PAHs, and the relationships among these components. Seasonal variations of  
112 different PM<sub>2.5</sub> components were also discussed. Furthermore, we employed an  
113 Aerodyne soot particle aerosol mass spectrometer (SP-AMS) (Onasch et al., 2012;Lee et  
114 al., 2015;Wang et al., 2016c) to investigate the properties and potential sources of OA  
115 on the basis of high resolution mass spectra determined by the SP-AMS. Findings from  
116 this study also add knowledge to the framework of Pan-Eurasian Experiment (PEEX)  
117 (Kulmala et al., 2015).

## 118 2. Experiments

### 119 2.1. Sampling site and PM<sub>2.5</sub> collection

120 The sampling site was set on the rooftop of a nine-story building inside the campus of  
121 Jiangsu University of Technology in Changzhou (31.7°N, 119.9°E), as shown in Fig. 1.  
122 This site locates in the southwestern part of Changzhou, surrounded by a residential area,  
123 approximately 0.5 km away from an urban street - Zhongwu Road, and has no direct  
124 influences from industrial emissions (14.7 km away from the closest industrial plant –  
125 Bao Steel). Meteorological parameters including temperature, relative humidity (RH),  
126 wind speed (WS), wind direction (WD), and concentrations of gas-phase species such as  
127 SO<sub>2</sub> and NO<sub>2</sub> are recorded by the air quality monitoring station inside the campus, which  
128 is about 500 meters away from the site. The average meteorological parameters of four  
129 seasons are shown in Table 1. The wind rose plots of different seasons are shown in Fig.  
130 S1 in the supplement. The wind speed was generally low in Changzhou (on average, 1.1,  
131 1.6, 0.9 and 0.9 m s<sup>-1</sup> in spring, summer, fall and winter, respectively).

132 PM<sub>2.5</sub> were collected onto 90 mm quartz fiber filters (Whatman, QM-A) using a  
133 medium volume sampler (TH-150 C, Wuhan Tianhong Ltd., China) with a flow rate of  
134 100 L min<sup>-1</sup>. The filters, wrapped in aluminum foil, were prebaked at 450 °C for 4 hours  
135 prior to sampling. The sampler began to collect particles at 9:00 am and stopped at 5:00  
136 am of the following day, ensuring the duration time for each sample of 20 hours. A total  
137 of 69 PM<sub>2.5</sub> samples were collected: 20 July - 19 August 2015 (summer, 11 samples), 18  
138 September - 25 October 2015 (fall, 23 samples), 7 December 2015 - 15 January 2016  
139 (winter, 24 samples) and 1 March - 12 April 2016 (spring, 11 samples).

140 Before and after sampling, the filters were conditioned under constant temperature  
141 (22±1°C) and relative humidity (45±5%) for 48 h and weighted by a microbalance  
142 (precision of 0.01 mg). The filters were then wrapped and sealed in aluminum foil  
143 envelopes separately, stored in a freezer at -20 °C until. Note filter-based measurements  
144 are inevitably subjected to various sampling artifacts including evaporation of  
145 semi-volatile species, and absorption of gases. Nitrate in the form of ammonium nitrate  
146 may have some evaporation loss as it is sensitive to temperature variations during

147 sampling, and absorption of gases may influence the quantification of particle-bound  
148 polycyclic aromatic hydrocarbons (PAHs).

149

## 150 **2.2 Chemical analysis**

### 151 **2.2.1 IC analysis**

152 One quarter of a filter was put into a glass tube and 25 mL deionized water (18.2  
153 MΩ cm<sup>-1</sup>) was then added. After 15 min ultrasonic extraction, the solution was filtrated  
154 through an acetate-cellulose filter with 0.45 μm pore size. Concentrations of the WSIs  
155 in the aqueous extract, including five anions (F<sup>-</sup>, Cl<sup>-</sup>, NO<sub>2</sub><sup>-</sup>, NO<sub>3</sub><sup>-</sup>, SO<sub>4</sub><sup>2-</sup>) and five  
156 cations (Na<sup>+</sup>, NH<sub>4</sub><sup>+</sup>, K<sup>+</sup>, Mg<sup>2+</sup>, Ca<sup>2+</sup>), were then measured by the ion chromatograph (IC,  
157 Dionex ICS-600 for anions and ICS-1500 for cations). The method detection limits  
158 (MDLs) were determined to be 18.0, 7.3, 5.2, 6.3, 11.0, 18.7, 3.3, 4.6, 2.6, and 11.5 μg  
159 L<sup>-1</sup> for F<sup>-</sup>, Cl<sup>-</sup>, NO<sub>2</sub><sup>-</sup>, NO<sub>3</sub><sup>-</sup>, SO<sub>4</sub><sup>2-</sup>, Na<sup>+</sup>, NH<sub>4</sub><sup>+</sup>, K<sup>+</sup>, Mg<sup>2+</sup> and Ca<sup>2+</sup>, respectively, and all  
160 measured concentrations were above the MDLs. Note the filter blanks were treated in  
161 the same way, and all data for the samples reported here were blank corrected, other  
162 analyses in the following sections were also blank corrected unless specified. The  
163 concentrations of all measured species in PM<sub>2.5</sub> sample were also converted to μg m<sup>-3</sup>  
164 based on the measured concentrations and the air volume pulled through the filter. The  
165 uncertainty of the IC measurements, calculated as three times the standard deviation of  
166 replicate measurements of blank filters, is shown in Table 2.

167

### 168 **2.2.2 ICP-OES analysis**

169 Another quarter of a filter was cut and placed in a Teflon vessel, digested with 10  
170 mL mixture of HNO<sub>3</sub>-HCl (1:1, v:v) in a microwave system (XT-9900A, Shanghai  
171 Xintuo Co.) for 45 minutes. After the digested solution cooled down to room  
172 temperature, it was filtered through a 0.45 μm acetate-cellulose filter. The filtrate was  
173 then diluted using deionized water to 50 mL, and analyzed using Optima 8000 (Perkin  
174 Elmer, USA) inductively coupled plasma optical emission spectrometry (ICP-OES) to  
175 determine concentrations of eight trace elements (Mn, Zn, Al, B, Cr, Cu, Fe, Pb). It is

176 worth to mention that we also tried to measure the concentrations of other trace elements  
177 such as Ti, Ni, Ba, but found they were mostly below the detection limits thus were not  
178 included in this work. All samples were determined in a triplicate, and a difference  
179 within 5% was considered acceptable. Measurement uncertainties for trace metals were  
180 in the range of 10.3 – 18.5%, with an average of 16.3% (Table 2).

181

### 182 **2.2.3 OC/EC and WSOC analysis**

183 Analysis procedure of OC/EC was similar to a previous study (Zhao et al., 2015) .  
184 Briefly, OC and EC were measured by the DRI model 2001 thermal/optical carbon  
185 analyzer (Atmoslytic Inc. Calabasas, CA) using a 0.526 cm<sup>2</sup> filter punch for each sample,  
186 following the IMPROVE TOR protocol (Chow et al., 2004). Filter was measured  
187 stepwise at temperatures of 140 °C (OC<sub>1</sub>), 280 °C (OC<sub>2</sub>), 480 °C (OC<sub>3</sub>), and 580 °C  
188 (OC<sub>4</sub>) under a helium atmosphere, and 580 °C (EC<sub>1</sub>), 740 °C (EC<sub>2</sub>), and 840 °C (EC<sub>3</sub>)  
189 under a 2% oxygen/98% helium atmosphere. OC is calculated as OC<sub>1</sub> + OC<sub>2</sub> + OC<sub>3</sub> +  
190 OC<sub>4</sub> + OP and EC as EC<sub>1</sub> + EC<sub>2</sub> + EC<sub>3</sub> – OP, where OP is the optical pyrolyzed OC. The  
191 detection limit of OC was estimated to be 30-80 ng m<sup>-3</sup> and EC was ~30 ng m<sup>-3</sup> based on  
192 a previous study (Mirante et al., 2014).

193 The WSOC concentrations were determined by a TOC analyzer (TOC-L, Shimazu,  
194 Japan) using a thermos-catalytic oxidation approach. Instrument details and procedure of  
195 the WSOC analysis can be found in our previous work (Ge et al., 2014). The MDL was  
196 5.0 µg L<sup>-1</sup> and measurement uncertainties ranged from 3.4 - 6.0%.

197

### 198 **2.2.4 GC-MS analysis for particulate PAHs**

199 Due to the limitation of samples, we only analyzed PAHs for spring and winter  
200 samples. The analysis was conducted following the standard procedure, similar to the  
201 work of Szabó et al. (2015). One quarter of a filter was treated by Soxhelt extraction for  
202 18 hours using 250 mL mixture of *n*-hexane/ethylether (5:1, v/v). To determine the  
203 recovery rates, 100 ng of deuterated surrogate standard solution containing  
204 naphthalene-d<sub>8</sub> and perylene-d<sub>12</sub> (o2si, USA) was added into the sample prior to

205 extraction, and the average recovery rates of d<sub>8</sub> and d<sub>12</sub> were over 90%. The extracts  
206 were then concentrated to about 2 mL by a rotary evaporator, purified in a  
207 chromatography column (filled with 3 cm deactivated Al<sub>2</sub>O<sub>3</sub>, 10g silica gel, 2 cm  
208 deactivated Na<sub>2</sub>SO<sub>4</sub>). The column was first eluted with 25 mL *n*-hexane and the eluate  
209 was discarded, then elution was carried out using 30 mL dichloromethane/*n*-hexane  
210 (1:1,v:v). Samples containing PAHs were again concentrated to about 2 mL by the  
211 rotary evaporation. Finally they were condensed to exactly 1 mL under a gentle N<sub>2</sub>  
212 steam in a 60 °C water bath. The extracts are transferred into ampoule bottles and stored  
213 in a refrigerator until analysis.

214 The PAH compounds in the final extracts were analyzed with a gas  
215 chromatography - mass spectrometer (GC-MS) (Agilent 7890-7000B, USA), using a  
216 DB-5ms capillary column (30 m×0.25 mm×0.5 μm). The instrument conditions were  
217 set as follows: injector at 200 °C; ion source at 230 °C; the column was programmed at  
218 40 °C for 2 min, then increased to 100 °C at a rate of 10 °C min<sup>-1</sup>, held for 1 min, then  
219 increased to 250 °C at 20 °C min<sup>-1</sup>, and finally held for 3 min at 250 °C. The mass  
220 selective detector was operated in the electron impact mode using 70 eV. Multi reaction  
221 monitor modes were employed for the identification and quantification of PAHs.

222 Before sample analysis, calibration standards at a series of concentrations were  
223 prepared from aromatic hydrocarbon standard (O2si, USA) containing 18 PAH  
224 compounds (1000 mg L<sup>-1</sup>), which are naphthalene (NaP) (C<sub>10</sub>H<sub>8</sub>), acenaphthylene (Acy)  
225 (C<sub>12</sub>H<sub>8</sub>), acenaphthene (Ace) (C<sub>12</sub>H<sub>10</sub>), fluorene (Flu) (C<sub>13</sub>H<sub>10</sub>), phenanthrene (Phe)  
226 (C<sub>14</sub>H<sub>10</sub>), anthracene (Ant) (C<sub>14</sub>H<sub>10</sub>), fluoranthene (Flua) (C<sub>16</sub>H<sub>10</sub>), pyrene (Pyr) (C<sub>16</sub>H<sub>10</sub>),  
227 benzo(a)anthracene (BaA) (C<sub>18</sub>H<sub>12</sub>), chrysene (Chr) (C<sub>18</sub>H<sub>12</sub>), benzo(b)fluoranthene  
228 (BbF) (C<sub>20</sub>H<sub>12</sub>), benzo(k)fluoranthene (BkF) (C<sub>20</sub>H<sub>12</sub>), benzo(a)pyrene(BaP) (C<sub>20</sub>H<sub>12</sub>),  
229 Benzo(e)pyrene (BeP) (C<sub>20</sub>H<sub>12</sub>), benzo(j)fluoranthene (BjF) (C<sub>20</sub>H<sub>12</sub>), benzoperylene  
230 (BghiP) (C<sub>22</sub>H<sub>12</sub>), indeno(1,2,3-cd)pyrene (C<sub>22</sub>H<sub>12</sub>), and dibenz(a,h)anthracene (C<sub>22</sub>H<sub>14</sub>).  
231 These PAHs can be classified by the number of aromatic rings and molecular weights:  
232 low molecular weight (LMW) PAHs containing 2- and 3-rings (NaP, Acy, Ace, Flu, Phe,  
233 Ant), medium molecular weight (MMW) PAHs containing 4-rings (Flua, Pyr, BaA, Chr)



234 and high molecular weight (HMW) PAHs containing 5- and 6-rings (BbF, BkF, BjF,  
235 BaP, BeP, InP, DBA, BghiP) (Wang et al., 2015;Kong et al., 2015). The calibration was  
236 conducted twice prior to analysis. Identification and quantification of each PAH is based  
237 on its retention time and peak areas in the calibration curve and sample curve, and the  
238 total PAH concentration ( $\Sigma$  PAH) was calculated as the sum of concentrations of all 18  
239 individual PAHs. Figure S2 shows examples of the GC-MS spectra of a few 18-PAHs  
240 standards and two surrogate standards ( $d_8$  and  $d_{12}$ ).

241

### 242 **2.2.5 Offline SP-AMS analysis**

243 The Aerodyne AMS is specially designed for online and real-time measurements of  
244 the submicron aerosol particles. The instrument has a very fine time resolution thus is  
245 powerful in capturing the quick atmospheric processes occurred in real atmosphere.  
246 While in this study, we used the SP-AMS for offline filter sample analyses. Compared  
247 with the online measurements, there are a few advantages: 1) it can greatly expand the  
248 application of AMS because it is often unrealistic to deploy the AMS for very long  
249 periods as it requires highly skilled personal to carefully maintain and operate the  
250 instrument; 2) for some sites, it is not accessible or not suitable for AMS deployment; 3)  
251 AMS analysis of organics can provide more details, for instance the elemental  
252 composition, oxidation states, etc., thus can offer useful insights into the origin of OA; 4)  
253 offline analyses may introduce artifacts compared with the online measurements, but on  
254 the other hand, it also expands the size range as online measurements were often limited  
255 in submicron meter range.

256 The SP-AMS analysis procedure for offline filters was similar to that of Xu et al.  
257 (2013). Briefly, for each sample, 1/4 filter was extracted in 25 mL deionized water. The  
258 liquid extracts were aerosolized using an atomizer (TSI, Model 3076), and the mist  
259 passed through a silica-gel diffusion dryer, leaving dry particles which were  
260 subsequently analyzed by the SP-AMS. Note the SP-AMS was operated with the laser  
261 off so similar to other AMS measurements; it measured non-refractory organic species  
262 that can vaporize fast at the oven temperature of 600 °C. The instrument employs the 70

263 eV electron impact (EI) ion generation scheme, all vaporized species were broken into  
264 ion fragments with specific mass-to-charge ( $m/z$ ) ratios, and the time-of-flight mass  
265 spectrometer outputs the mass spectrum that records the ions according to their signal  
266 intensities at different  $m/z$  ratios. Ion fragments with  $m/z$  up to 300 amu were recorded in  
267 this study. The SP-AMS mass spectra can well represent the total OA constituents, and  
268 the bulk OA properties such as elemental ratios including oxygen-to-carbon (O/C),  
269 hydrogen-to-carbon (H/C) and nitrogen-to-carbon (N/C) ratios, and the organic  
270 mass-to-organic carbon (OM/OC) ratio can be obtained. Note although the SP-AMS is  
271 limited in molecular-level speciation analysis (Drewnick, 2012), some compounds can  
272 be identified via recognition of their corresponding fingerprint ions, and particular  
273 sources can be separated and quantified via further factor analyses.

274 The SP-AMS data were processed using the Igor-based software toolkit  
275 SQUIRREL (version 1.56D) and PIKA (version 1.15D) (downloaded from:  
276 <http://cires.colorado.edu/jimenez-group/ToFAMSResources/ToFSoftware/index.html>),  
277 and the analysis procedure was similar to our previous work (Ge et al., 2012b). We did  
278 some minor modifications on the fragment table. For example, we set the organic  $\text{CO}_2^+$   
279 signal equal to organic  $\text{CO}^+$ , same as Aiken et al. (2008), as the  $\text{CO}_2^+$  signal in  $\text{PM}_{2.5}$   
280 may come from carbonate not organics, and since we used Argon as carrier gas so  
281 different from ambient measurements, the  $\text{CO}^+$  signal can be well separated and  
282 quantified from  $\text{N}_2^+$  at  $m/z$  28 (example shown in Fig. S3). Note the scatter plot of  
283 original  $\text{CO}_2^+$  vs.  $\text{CO}^+$  signals yielded a slope of 2.24. A recent AMS study using argon  
284 as carrier gas on  $\text{PM}_1$  filter samples also showed systematically higher  $\text{CO}_2^+$  signal than  
285  $\text{CO}^+$  but much less than the factor of 2.24, indicating that  $\text{CO}_2^+$  signal from  $\text{PM}_{2.5}$  sample  
286 was influenced by  $\text{CO}_2^+$  from carbonate. Accordingly, organic  $\text{H}_2\text{O}^+$ ,  $\text{HO}^+$ ,  $\text{O}^+$  were  
287 scaled to  $\text{CO}_2^+$  using the ratios proposed by Aiken et al. (2008), and the elemental  
288 compositions and H/C, N/C, O/C and OM/OC ratios of OA reported in this study were  
289 determined according to the method of Canagaratna et al. (2015).

290

### 291 **2.3 Determination of WSOA, WIOA**

292 Mass concentrations of WSOA were calculated by multiplying the WSOC  
293 concentrations determined from the TOC analyzer with the OM/OC ratios calculated  
294 from the SP-AMS mass spectra (Fig. 2) (equation 1). As shown in Fig. 2, most OM/OC  
295 values were within the range of 1.5-2.3, in consistent with the typical OM/OC ratios  
296 observed at other urban sites. However, the O/C and OM/OC ratios have no significant  
297 seasonal differences, indicating that the WSOA sources were likely similar.

298 The water-insoluble organic carbon (WIOC) mass was calculated as the difference  
299 between the OC determined by the OC/EC analyzer and the WSOC, and a factor of 1.3  
300 suggested by Sun et al. (2011a), was used to convert the WIOC mass to the mass of  
301 water-insoluble organic aerosol (WIOA) (equation 2). The total organic aerosol (OA)  
302 was treated as the sum of WSOA and WIOA (equation 3).

$$303 \quad \text{WSOA} = \text{WSOC} \times \text{OM/OC}_{\text{WSOA}} \quad (1)$$

$$304 \quad \text{WIOA} = (\text{OC} - \text{WSOC}) * 1.3 \quad (2)$$

$$305 \quad \text{OA} = \text{WSOA} + \text{WIOA} \quad (3)$$

306 The measurement uncertainty of WSOA was calculated as the sum of squares of  
307 uncertainties of OM/OC ratios and WSOC, ranging from 6.9 - 8.5% (Table 2).

308

## 309 **2.4 Source apportionment of WSOA**

310 In this work, we used the PMF Evaluation Toolkit v 2.06 (Ulbrich et al., 2009) and  
311 followed the protocol described by Zhang et al. (2011) to conduct the PMF analyses.  
312 Typically, inclusion of more samples can provide better PMF results and more  
313 scientifically sound interpretation of the sources. But applications of PMF model on a  
314 limited number of samples (much less than 100) were also reported previously (e.g.,  
315 Huang et al., 2014; Sun et al., 2011a), and proven to be able to provide very valuable  
316 insights into the sources of OA.

317 Prior to PMF execution, the following steps were performed: Data and error matrix  
318 for WSOA were first adjusted based on equation 1; ions with low signal-to-noise (S/N <  
319 0.2) were removed, and ions with S/N ratios between 0.2 and 2 were downweighted by a  
320 factor of 2; Two runs with huge mass loading spikes were removed; all isotopic ions

321 were removed since their signals are not measured directly but scaled to their parent ions.  
322 The PMF solutions were explored by varying the factors from 1 to 8 and the rotational  
323 forcing parameter ( $f_{\text{peak}}$ ) from  $-1$  to  $1$  with an increment of  $0.1$ . The four-factor  
324 solution with  $f_{\text{peak}}=0$  was chosen as the best solution. The mass spectra of three-factor  
325 and five-factor solutions were presented in Fig. S4. The three-factor solution does not  
326 resolve well the oxygenated OA factors as many oxygenated ions were mixed with the  
327 primary OA factors. The five-factor solution splits a primary OA factor into two factors  
328 with very similar mass profiles. Also, by investigating the correlations of the factors  
329 with their corresponding tracer ions, and sulfate, nitrate, etc., of the 3-, 4-, and 5-factor  
330 solutions, the 4-factor solution was found to be the most reliable and representative  
331 solution.

332

### 333 **3. Results and discussion**

#### 334 **3.1 Overview of PM<sub>2.5</sub> concentrations and components**

335 The annual and seasonal average concentrations of PM<sub>2.5</sub>, OC, EC, OA, WSIs,  
336 trace elements and PAHs are summarized in Table 3. As shown in Table 3, the PM<sub>2.5</sub>  
337 concentrations (in  $\mu\text{g m}^{-3}$ ) were on average ( $\pm 1\sigma$ )  $106.0 (\pm 24.4)$ ,  $80.9 (\pm 37.7)$ ,  $103.3$   
338 ( $\pm 28.2$ ), and  $126.9 (\pm 50.4)$  in spring, summer, fall and winter, respectively, with annual  
339 average of  $108.3 (\pm 40.8)$ , comparable to the PM<sub>2.5</sub> concentrations in Nanjing ( $106 \mu\text{g}$   
340  $\text{m}^{-3}$  in 2011) (Shen et al., 2014), Tianjin ( $109.8 \mu\text{g m}^{-3}$  in 2008) (Gu et al., 2010) and  
341 Hangzhou ( $108.2 \mu\text{g m}^{-3}$  in 2004-2005) (Liu et al., 2015), but lower than that in Jinan  
342 ( $169 \mu\text{g m}^{-3}$  in 2010) (Gu et al., 2014). The PM<sub>2.5</sub> concentrations were highest in winter  
343 and relatively low in summer, similar to those found in most cities, such as Tianjin (Gu  
344 et al., 2010) and Hangzhou (Liu et al., 2015). Previous studies showed that low  
345 concentrations occurring in summer were mainly due to the relatively high boundary  
346 layer height, low RH and high temperature (Cheng et al., 2015; Huang et al., 2010). The  
347 temperatures and RH values were on average  $32.1 \text{ }^\circ\text{C}$  and  $61.1\%$  in summer during the  
348 observation period (Table 1). Overall, the daily average concentration of PM<sub>2.5</sub> during  
349 sampling period exceeds  $75 \mu\text{g m}^{-3}$  - the second-grade national air quality standard

350 (NAAQS)(GB 3095-2012), and on some heavily polluted days, the PM<sub>2.5</sub> mass loadings  
351 can even exceed 3 times the NAAQS standard.

352 Overall, the reconstructed PM<sub>2.5</sub> mass estimated by the sum of OA, EC and WSIs  
353 vs. gravimetrically determined PM<sub>2.5</sub> mass were shown in Fig. 3(a-d). The mass  
354 proportions of all measured components to the PM<sub>2.5</sub> mass are illustrated by five inserted  
355 pie charts representing four seasons and the whole year, respectively. On average, the  
356 quantified species can occupy 78.6% of the PM<sub>2.5</sub> mass (note trace elements and PAHs  
357 were not included as they were only determined for partial samples), and the mass  
358 closure appears to be better for spring and winter samples. Overall, our results are  
359 similar to some previous results, such as in Beijing (68%) (Zhang et al., 2013). Details  
360 and characteristics of individual components are discussed in the following sections.

361

### 362 **3.2 Water soluble inorganic ions**

363 The average concentrations ( $\pm\sigma$ ) of total WSIs were 66.5 ( $\pm 17.2$ ), 35.0 ( $\pm 20.2$ ),  
364 51.0 ( $\pm 17.2$ ), and 66.8 ( $\pm 23.6$ )  $\mu\text{g m}^{-3}$  in spring, summer, fall and winter, respectively,  
365 with an annual average of 56.4 ( $\pm 22.9$ )  $\mu\text{g m}^{-3}$ . The level was lowest in summer likely  
366 due to the conditions favorable for pollutants dispersion and the wet scavenging of these  
367 ions under summer monsoon circulation and precipitation. In total, all WSIs can  
368 account for 62.7%, 43.2%, 49.3% and 52.6% of PM<sub>2.5</sub> in spring, summer, fall and winter,  
369 respectively, with the annual average WSIs/PM<sub>2.5</sub> percentage of 52.1%, a little higher  
370 than the previously reported value of 45.3% in Handan in 2013 (Meng et al., 2016).

371 The mass fractions of individual ions to total WSIs followed the order: NO<sub>3</sub><sup>-</sup>  
372 (34.2%) > SO<sub>4</sub><sup>2-</sup> (31.0%) > NH<sub>4</sub><sup>+</sup> (21.2%) > Cl<sup>-</sup> (6.0%) > Na<sup>+</sup> (3.8%) > K<sup>+</sup> (1.8%) > Ca<sup>2+</sup>  
373 (1.2%) > Mg<sup>2+</sup> (0.3%) > NO<sub>2</sub><sup>-</sup> and F<sup>-</sup> (0.2%) (Fig. 4b). Secondary inorganic ions  
374 including SO<sub>4</sub><sup>2-</sup>, NO<sub>3</sub><sup>-</sup>, and NH<sub>4</sub><sup>+</sup>, constitute the majority of WSIs (86.4%) (Fig. 4b)  
375 with the highest one being NO<sub>3</sub><sup>-</sup>. Nitrate and ammonium concentrations displayed  
376 distinct seasonal variations - highest in spring (NO<sub>3</sub><sup>-</sup>: 26.4  $\mu\text{g m}^{-3}$ , NH<sub>4</sub><sup>+</sup>: 14.8  $\mu\text{g m}^{-3}$ ),  
377 following by winter (24.1 and 13.1  $\mu\text{g m}^{-3}$ ), and lowest in summer (6.8 and 8.2  $\mu\text{g m}^{-3}$ ).  
378 On the other hand, as a non-volatile species, sulfate concentrations showed no obvious

379 seasonal differences.

380 The cross-correlation relationships between different ions can be used to infer their  
381 possible common sources. Figure 5 shows the Pearson's correlation coefficients ( $r$ )  
382 between ions for four seasons, respectively. As illustrated,  $\text{NH}_4^+$  had good correlations  
383 with  $\text{SO}_4^{2-}$  and  $\text{NO}_3^-$  ( $r > 0.70$ ), and particularly high  $r$  values were found in winter (with  
384  $\text{SO}_4^{2-}$ :  $r = 0.90$ , with  $\text{NO}_3^-$ :  $r = 0.96$ ) and summer (with  $\text{SO}_4^{2-}$ :  $r = 0.98$ , with  $\text{NO}_3^-$ :  $r =$   
385  $0.93$ ), indicating these three ions were mainly present in the form of ammonium nitrate  
386 and ammonium sulfate. Moreover, the correlations between  $\text{Na}^+$  and  $\text{Cl}^-$  varied largely  
387 with the seasons, poor in summer ( $r = -0.19$ ) and winter ( $r = 0.37$ ), indicating different  
388 sources for them. For chloride, the annual average  $\text{Cl}^-/\text{Na}^+$  mass ratio was 1.58, larger  
389 than 1.17 in seawater (Zhang et al., 2013), indicating the important contributions from  
390 anthropogenic activities to chloride (such as coal combustion) in Changzhou, in  
391 particular in winter as the content of  $\text{Cl}^-$  in winter was significantly elevated. By contrast,  
392  $\text{K}^+$  and  $\text{Cl}^-$  have good correlations ( $r$  of 0.86, 0.76, 0.80 and 0.62 in spring, summer, fall  
393 and winter), suggesting that  $\text{K}^+$  may co-emit with chloride. According to correlation  
394 analysis in Fig. 5,  $\text{Mg}^{2+}$  and  $\text{Ca}^{2+}$  had good relations with  $r$  of 0.58, 0.80, 0.81 and 0.78  
395 in spring, summer, fall and winter, respectively, indicating a similar source likely crustal  
396 material for these two ions.

397 Acidity of  $\text{PM}_{2.5}$  can be evaluated by AE (anion equivalence) vs. CE (cation  
398 equivalence), which is calculated by converting the concentrations of anions and cations  
399 ( $\mu\text{g m}^{-3}$ ) into molar concentrations ( $\mu\text{mol m}^{-3}$ ) using the following equations.

$$400 \quad \text{AE} = \frac{\text{SO}_4^{2-}}{48} + \frac{\text{NO}_3^-}{62} + \frac{\text{NO}_2^-}{46} + \frac{\text{Cl}^-}{35.5} + \frac{\text{F}^-}{19} \quad (4)$$

$$401 \quad \text{CE} = \frac{\text{NH}_4^+}{18} + \frac{\text{Mg}^{2+}}{12.2} + \frac{\text{Ca}^{2+}}{20} + \frac{\text{K}^+}{39} + \frac{\text{Na}^+}{23} \quad (5)$$

402

403 Figure 6a illustrates the scatter plots of CE vs. AE in four seasons. The slopes were 1.18,  
404 1.09, 1.03 and 0.93 in spring, summer, fall and winter, respectively, indicating the  
405 particles are generally neutralized. Normally, the ratio of  $\text{NH}_4^+_{\text{meas}}/\text{NH}_4^+_{\text{pred}}$ , proposed  
406 by Zhang et al. (2007b), can be used to evaluate the existing form of  $\text{NH}_4^+$  ion. The  
407 predicted  $\text{NH}_4^+$  ( $\text{NH}_4^+_{\text{pred}}$ ) was calculated using Equation 6.

$$NH_4^+_{pred} = 18 \times \left( 2 \times \frac{SO_4^{2-}}{96} + \frac{NO_3^-}{62} + \frac{Cl^-}{35.5} \right) \quad (6)$$

Figure S5 illustrated the ratio of  $NH_{4meas}^+/NH_{4pred}^+$  in  $PM_{2.5}$  during four seasons. As presented, the ratios were 0.95, 0.93, 0.87, 0.75 in spring, summer, fall and winter, respectively, again verifying that  $(NH_4)_2SO_4$  and  $NH_4NO_3$ ,  $NH_4Cl$  were dominant forms for these ionic species.

In addition, the mass ratio of  $NO_3^-$  to  $SO_4^{2-}$  ( $NO_3^-/SO_4^{2-}$ ) can be used to determine whether mobile sources (vehicle) or stationary sources (coal combustion) are dominant for these ions (Wang et al., 2006b; Arimoto et al., 1996). When the  $NO_3^-/SO_4^{2-}$  mass ratio exceeds 1, it means that particle sources at the observation site are likely dominated by mobile sources, while fixed sources play major roles when the ratio is below 1. In this study, the mass ratios of  $NO_3^-/SO_4^{2-}$  were 1.52, 0.43, 0.99 and 1.29 in the spring, summer, fall and winter, respectively, with an annual average ratio of 1.21 (Fig. 6b). The  $NO_3^-/SO_4^{2-}$  ratio varied largely with seasons. Note in summer, a lower  $NO_3^-/SO_4^{2-}$  ratio may be also ascribed to high temperature which leads to the evaporation of  $NH_4NO_3$ , yet the high  $NO_3^-/SO_4^{2-}$  in winter and spring is more likely relevant to traffic emissions from Zhongwu Road near the sampling site (Fig. 1).

Previous studies (Xu et al., 2014) have indicated that nitrogen oxidation ratio (NOR =  $nNO_3^-/(nNO_3^-+nNO_2)$ ,  $n$  refers to the molar concentration), and sulfur oxidation ratio (SOR =  $nSO_4^{2-}/(nSO_4^{2-}+nSO_2)$ ), can be used to estimate the transformation of  $NO_2$  and  $SO_2$  to particle-phase  $NO_3^-$  and  $SO_4^{2-}$ . The larger SOR and NOR mean more secondarily formed nitrate and sulfate. The seasonal values for SOR and NOR are plotted in Fig. 6 (c-d). On average, the SOR value appeared to be a bit higher in summer, indicating that strong photochemical oxidation for sulfate formation, while NOR is relatively higher in spring, suggesting conversion of  $NO_x$  into nitrate is more efficient in spring in Changzhou.

433

### 434 3.3 Trace elements

435 Eight trace elements (Mn, Zn, Al, B, Cr, Cu, Fe, Pb) for samples collected during

436 fall and winter were determined in this study. The average concentrations ( $\mu\text{g m}^{-3}$ ) are  
437 shown in Fig. 7a. The total concentrations were  $6.38 \mu\text{g m}^{-3}$  and  $2.77 \mu\text{g m}^{-3}$ , accounting  
438 for 5.0% and 2.7% of the total  $\text{PM}_{2.5}$  mass during winter and fall, respectively. These  
439 values were relatively higher than those in other cities in China, such as 1.74% - 2.04%  
440 in Hangzhou (Liu et al., 2015). This probably can be explained by re-suspended dust  
441 from building construction around the site during the sampling period. In this study, the  
442 observed mean levels of trace elements in fall were in the order of  
443  $\text{Fe} > \text{Zn} > \text{B} > \text{Al} > \text{Cu} > \text{Mn} > \text{Pb} > \text{Cr}$ , and ranked in  $\text{Zn} > \text{Fe} > \text{B} > \text{Al} > \text{Cu} > \text{Mn} > \text{Pb} > \text{Cr}$  during  
444 winter (Fig. 7a). In fall, Fe accounted for 39.0% of the total trace metal mass, following  
445 by Zn (25.6%), B (12.3%) and Al (9.2%), while in winter Zn contributed the largest  
446 (53.7%), following by Fe and B. Overall, Fe and Zn were the two most abundant trace  
447 elements in  $\text{PM}_{2.5}$ , accounting for over half of the trace metal mass. Previous work also  
448 found that mass loading of Zn was higher than other elements, even higher than Al in  
449 Nanjing in 2013 (Qi et al., 2016b; Qi et al., 2016a). Vehicle exhaust is likely one major  
450 contributor to the high concentration of Zn.

451 In general, the correlations between various heavy metals are weak, as depicted in  
452 Fig. 7b-d, indicating that the complex sources including both natural and anthropogenic  
453 sources for the trace metals observed here. For instance, Cr, Cu, Pb, and Zn can be  
454 released from lubricating oils, tail pipe emissions, brake and tire wears (Zhang et al.,  
455 2013); Fe and Mg are primarily crustal elements, while Zn and Cu are mainly from  
456 anthropogenic sources. Fe and Al were only moderately correlated (for example, in fall  
457 with  $r=0.74$ , Fig. 7b), showing that they are not from exactly same sources.

458

### 459 **3.4 OC and EC**

460 As presented in Table 3, the annual average EC concentration in Changzhou was  
461  $5.4 \mu\text{g m}^{-3}$ , close to Nanjing ( $5.3 \mu\text{g m}^{-3}$ ) (Li et al., 2015) and Tianjin ( $5.9 \mu\text{g m}^{-3}$ ) (Gu et  
462 al., 2010), but lower than those in other cities (e.g.,  $22.3 \mu\text{g m}^{-3}$  in Beijing (Duan et al.,  
463 2012), and higher than that observed in Shanghai ( $2.8 \mu\text{g m}^{-3}$ ) (Feng et al., 2009). The  
464 seasonally averaged OC concentrations were highest in winter ( $18.3 \mu\text{g m}^{-3}$ ), followed



465 by fall ( $13.2 \mu\text{g m}^{-3}$ ) and spring ( $11.2 \mu\text{g m}^{-3}$ ), and lowest in summer ( $7.9 \mu\text{g m}^{-3}$ ). The  
466 annual average OC concentration was  $13.8 \mu\text{g m}^{-3}$ , comparable to those measured in  
467 other cities, such as Shanghai ( $14.7 \mu\text{g m}^{-3}$ )(Feng et al., 2009), and Tianjin ( $16.9 \mu\text{g m}^{-3}$ )  
468 (Gu et al., 2010).

469 The mass concentrations of total carbon (TC, the sum of OC and EC) were 16.0,  
470 12.1, 21.0,  $22.3 \mu\text{g m}^{-3}$  in spring, summer, fall and winter, respectively (Table 2),  
471 corresponding mass contributions to  $\text{PM}_{2.5}$  were 15.0%, 15.0%, 20.3%, and 17.6% with  
472 an annual mean of 17.8%. This value was similar to those measured in other cities in  
473 China, such as Jinan (10 - 15%)(Gu et al., 2014), Shanghai (15%) (Zhao et al., 2015),  
474 and other cities (10 - 15% in Tianjin, Haining, Zhongshan and Deyang; Zhou et al.  
475 (2016)). The OA concentrations exhibited similar seasonal variations as  $\text{PM}_{2.5}$ , and  
476 ranked in the order: winter ( $31.2 \pm 11.9$ ) > fall ( $21.6 \pm 11.9$ ) > spring ( $18.9 \pm 4.1$ ) > summer  
477 ( $14.0 \pm 1.4$ ). The average mass fraction of OA in  $\text{PM}_{2.5}$  was 21.5%, and the WSOA  
478 contributed 77.7% of the total OA mass, similar to the results in Atlanta (approximately  
479 88% in rural Centreville and 77% in urban Atlanta) (Xu et al., 2017).

480

481 As illustrated in Fig. 8, the OC/EC ratios varied in different seasons and were  
482 largest in winter (5.16) followed by spring (2.38), summer (1.88) and fall (1.75). The  
483 largest OC/EC ratio occurred in winter, indicating that secondary organic carbon (SOC)  
484 was likely a significant component of  $\text{PM}_{2.5}$  in winter (Chow et al., 2005), however, the  
485 high OC/EC ratio may be influenced by biomass burning and/or coal combustion  
486 emissions during wintertime too. A number of previous studies about the carbonaceous  
487 aerosols in the YRD region also showed that highest OC/EC ratio occurred in winter and  
488 the ratio was often larger than 2, such as Shanghai (6.35) (Zhao et al., 2015), Nanjing  
489 (2.8)(Li et al., 2015), in consistent with our current results in Changzhou.

490

### 491 **3.5 Particulate PAHs analysis with GC-MS and SP-AMS**

492 The average concentrations of the 18 individual PAH and total PAHs ( $\Sigma\text{PAHs}$ ) in  
493 winter and spring are listed in Table 4. It can be seen that InP (% of total PAHs: 12.6 -  
494 14.8%), BghiP (10.8 - 12.3%) and Chr (10.4 - 11.0%) were the three most abundant

495 PAHs species, followed by BbF (8.69 - 9.39%), BaP (7.37 - 8.29%), BeP (5.83 - 8.61)  
496 and BaA (4.53 - 8.27%). The  $\Sigma$ PAHs in PM<sub>2.5</sub> were found in the range of 14.0 - 365.7  
497 ng m<sup>-3</sup> (mean: 140.25 ng m<sup>-3</sup>) and 8.9 - 91.3 ng m<sup>-3</sup> (mean: 41.42 ng m<sup>-3</sup>) during winter  
498 and spring, respectively. The  $\Sigma$ PAHs concentrations in this study are higher than those  
499 reported in Zhenzhou (39 and 111 ng/m<sup>3</sup> in spring and winter)(Wang et al., 2014) and  
500 Shanghai (13.7 ng m<sup>-3</sup> in spring) (Wang et al., 2015), but lower than that reported in  
501 Liaoning Province (75 - 1900 ng m<sup>-3</sup>) (Kong et al., 2010). PAHs with medium (4 rings)  
502 and high molecular weights (5 - 6 rings) (MMW and HMW) occupied the majority of  
503 PAHs (88.9% in winter and 79.4% in spring). It is well known that MMW and HMW  
504 PAHs are usually associated with coal combustion and vehicular emissions (Wang et al.,  
505 2015). Prior study in Nanjing (He et al., 2014) also showed the significant contribution  
506 of traffic exhaust to some PAHs including BbF, Chr, Flu, InP, BeP, and BghiP, which in  
507 total accounted for more than 53% of the total PAHs.

508 The diagnostic ratios of selected PAHs including Phe/(Ant+Phe), BaP/BghiP,  
509 Flua/(Flua+Pyr), BaP/(BaP+Chr) and Phe/(Ant+Phe) can be used to further distinguish  
510 the emission sources of PAHs (Szabó et al., 2015). As suggested previously (Feng et al.,  
511 2015; Saldarriaga-Noreña et al., 2015), traffic source was characterized with a ratio of  
512 BaP/BghiP > 0.6, and ratios of Flua/(Flua+Pyr) < 0.4, 0.4-0.5, > 0.5 suggest sources of  
513 petrogenic, fossil fuel combustion and coal/wood combustion, respectively. In this work,  
514 the BaP/BghiP of 0.61 (winter) and 0.76 (spring) and Flua/(Flua+Pyr) ratios of 0.47  
515 (winter) and 0.50 (spring), all suggest that local vehicular/fossil fuel combustion  
516 emissions could be a prominent contributor to particulate PAHs, and contribution from  
517 long-range transport was thus minor. Meanwhile, BaP/(BaP+Chr) ratio of 0.40 (winter )  
518 and 0.44 (spring) also point to the source of gasoline emission (Khalili et al., 1995).  
519 However, the Phe/(Ant+Phe) ratio of 0.89 (winter) and 0.86 (spring) indicate the coal  
520 combustion might be also an important source of PAHs.

521 On the other hand, by using the SP-AMS, we also identified a series of PAH ions,  
522 i.e., C<sub>16</sub>H<sub>10</sub><sup>+</sup> (*m/z* 202), C<sub>17</sub>H<sub>12</sub><sup>+</sup> (*m/z* 216), C<sub>18</sub>H<sub>10</sub><sup>+</sup> (*m/z* 226), C<sub>18</sub>H<sub>12</sub><sup>+</sup> (*m/z* 228), C<sub>19</sub>H<sub>12</sub><sup>+</sup>  
523 (*m/z* 240), C<sub>19</sub>H<sub>14</sub><sup>+</sup> (*m/z* 242), C<sub>20</sub>H<sub>10</sub><sup>+</sup> (*m/z* 250), C<sub>20</sub>H<sub>12</sub><sup>+</sup> (*m/z* 252), C<sub>21</sub>H<sub>12</sub><sup>+</sup> (*m/z* 264),

524  $C_{21}H_{14}^+$  ( $m/z$  266),  $C_{22}H_{12}^+$  ( $m/z$  276),  $C_{23}H_{12}^+$  ( $m/z$  288),  $C_{23}H_{14}^+$  ( $m/z$  290),  $C_{24}H_{12}^+$   
525 ( $m/z$  300),  $C_{24}H_{14}^+$  ( $m/z$  302),  $C_{25}H_{16}^+$  ( $m/z$  316),  $C_{26}H_{14}^+$  ( $m/z$  326), and  $C_{26}H_{16}^+$  ( $m/z$   
526 328)(Dzepina et al., 2007). Note many PAH ions identified by the SP-AMS were not  
527 measured by the GC-MS, and the PAH compound DBA which is determined by the  
528 GC-MS was not detected by the SP-AMS. This reflects the different sensitivities and  
529 responses to the particle-bound PAHs of these two techniques. Table 5 shows the  
530 correlation ( $r$ ) coefficients of the concentrations of a few selected PAHs, and the mass  
531 ratios of their concentrations measured by both the GC-MS and SP-AMS (results for  
532 SP-AMS were based on measurements of all samples, while results for GC-MS were for  
533 23 samples in winter and spring). It can be seen that the concentrations of  
534 GC-MS-determined PAHs correlated very well with each other ( $r > 0.92$ ), while the  
535 mass loadings determined by the SP-AMS correlated relatively weak. Also, the mass  
536 ratios determined from these two instruments were different. The inconsistencies may be  
537 due to the following reasons: (1) SP-AMS broke the parent PAH molecules into  
538 fragments due to 70 eV EI, thus concentration of a specific PAH ion from the SP-AMS  
539 cannot represent its corresponding parent PAH compound, while GC-MS determined the  
540 concentration of molecular PAH compound; (2) One PAH ion in the SP-AMS HRMS  
541 may be combination of a few PAHs compounds with the same molecular weights; (3)  
542 Sensitivities and responses to the different PAHs of the SP-AMS may be different, thus  
543 may lead to uncertainties of the PAHs quantification. Nevertheless, combining GC-MS  
544 and SP-AMS to improve the PAH measurements by the SP-AMS is valuable, and will  
545 be the subject of our future work.

546

### 547 **3.6 Source apportionment of WSOA**

#### 548 **3.6.1 WSOA mass spectral profile**

549 To gain further insights into the particulate OA characteristics, we performed the  
550 SP-AMS analyses on the water extract of the  $PM_{2.5}$  samples, with a focus on OA. The  
551 averaged high resolution mass spectra (HRMS) of WSOA classified by six ion  
552 categories and five elements are shown in Fig. 9, and the corresponding inset pie charts  
553 represent the mass percentages of the ion families and elements, respectively. As

554 illustrated in Fig. 9a, the  $C_xH_y^+$  ion family accounts for 386.2% of the WSOA HRMS,  
555 followed by  $C_xH_yO^+$  (28.5%),  $C_xH_yN_p^+$  (17.7%) and  $C_xH_yO_2^+$  (11.2%). It is worth to  
556 mention that we found that the  $C_xH_yN_p^+$  ions contributed significantly, and the organic N  
557 (ON) could occupy 6.4% of the total WSOA mass (Fig.9 b). The average concentration  
558 of water-soluble organic nitrogen (WSON) over the sampling period was  $1.16 \mu\text{g N m}^{-3}$   
559 ( $83.0 \text{ nmol N m}^{-3}$ ), which is in fact much lower than those measured in Beijing ( $226$   
560  $\text{nmol N m}^{-3}$ ) (Duan et al., 2009), Qingdao ( $129 - 199 \text{ nmol N m}^{-3}$ ) (Shi et al., 2010),  
561 Xi'an ( $300 \text{ nmol N m}^{-3}$ ) (Ho et al., 2015). The concentration of water-soluble inorganic  
562 nitrogen (WSIN, N from ammonium, nitrate and nitrite) was  $14.0 \mu\text{g N m}^{-3}$  base on  
563 Table 3, and thus the WSON content corresponds to 7.7% of water-soluble nitrogen  
564 (WSN = WSON + WSIN). This values is also much lower than those in Beijing (~30%)  
565 (Duan et al., 2009), Qingdao (19 - 22.6%), and Xi'an (22 - 68%) (Ho et al., 2015).

566 Nevertheless, the level of ON measured here are a few times higher than those  
567 observed in other locations from AMS measurements (typically 1 - 3%) (Xu et al., 2014),  
568 likely due to the following reasons: First, previous studies were online measurements on  
569 non-refractory submicron aerosols, while it is likely that the supermicron fine particles  
570 (1-2.5  $\mu\text{m}$ ) contain significant nitrogen-containing species, as observed before for  
571 marine aerosols (Violaki and Mihalopoulos, 2010). Secondly, we measured only the  
572 water-soluble fraction of OA, which may concentrate more nitrogen-containing species  
573 (partially from aqueous-phase processing). Thirdly, a recent study reveals that fossil fuel  
574 combustion-related emission can be a dominant source of ammonia in urban area (Pan et  
575 al., 2016), it thus can act as a significant contributor to amines as amines are often  
576 co-emitted with ammonia (Ge et al., 2011b); these amines can be neutralized by  
577 inorganic or organic acids and since aminium salts are highly hygroscopic (Ge et al.,  
578 2011a), they might be enriched in the WSOA, and generated significant  $C_xH_yN_p^+$  ions.  
579 Nevertheless, more AMS analyses on the water-extracted  $\text{PM}_{2.5}$  samples collected from  
580 other locations should be conducted to further verify the abundance of ON species in the  
581 AMS mass spectra of WSOA.

582 Overall, the average elemental ratios of the WSOA are 0.54 for O/C, 1.69 for H/C,

583 0.11 for N/C and 1.99 for OM/OC (Fig. 9a). WSOA is on average comprised of 50.2% C,  
584 7.1 % H, 36.1% O, 6.4% N and a negligible fraction (0.2%) of S (Fig. 9b).

585

### 586 **3.6.2 WSOA sources from PMF analysis**

587 The PMF analysis of the WSOA HRMS matrix identified four OA factors,  
588 including two primary OA (POA) factors, named as nitrogen-enriched hydrocarbon-like  
589 OA (NHOA), and local primary OA (LOA), and two secondary OA factors which are a  
590 less oxidized oxygenated OA (LO-OOA) and a more oxidized oxygenated OA  
591 (MO-OOA), as shown in Fig. 10.

592 The NHOA factor had a low O/C ratio (0.19), and was abundant in  $C_xH_y^+$  ions  
593 (33.8%) and the NHOA time series also varied closely with those ions, representing its  
594 features as traffic-related OA. In particular, the factor was rich in  $C_xH_yN_p^+$  ions (43.1%),  
595 as a result, it shows a much higher N/C ratio (0.26, Fig. 10a) than other factors, and  
596 correlated well with  $CHN^+$  ( $r = 0.91$ ),  $CH_4N^+$  ( $r = 0.95$ ),  $CH_2N^+$  ( $r = 0.85$ ), and  $C_2H_4N^+$   
597 ( $r = 0.87$ ) (Fig. 10b). The N-containing ions in the NHOA MS were dominated by the  
598 reduced ions ( $C_xH_yN^+$ ) rather than oxidized ones ( $C_xH_yO_zN^+$ ), suggesting that amino  
599 compounds were likely the major ON species, and was in consistent with our hypothesis  
600 aforementioned in Section 3.6.1 that they were mainly from fossil fuel combustion  
601 emissions. Nevertheless, future studies should be conducted to investigate in details the  
602 contribution of fossil fuel combustion to the atmospheric ON species.

603 Another primary OA factor was defined as a local primary OA (LOA) contains  
604 contributions from mixed anthropogenic emissions, such as cooking, coal combustion,  
605 etc. LOA had a low O/C ratio of 0.19 and also contained mainly reduced  $C_xH_y^+$  ions  
606 (60.8%) as well, verifying its primary origin. Note its mass profile is characterized by  
607 peaks at  $m/z$  55 (significant  $C_3H_3O^+$ ) and  $m/z$  57 (significant  $C_3H_5O^+$ ). The abundance of  
608  $C_3H_3O^+$  at  $m/z$  55 and  $C_3H_5O^+$  at  $m/z$  57 is a spectral feature of cooking OA, and the  
609 overall COA MS and O/C ratios are also similar to the COA factors reported in other  
610 studies, such as in Beijing. The LOA time series also correlated well with other  
611 cooking-related marker ions, such as  $C_5H_8O^+$  ( $r = 0.76$ ),  $C_6H_{10}O^+$  ( $r = 0.74$ ),  $C_7H_{12}O^+$  ( $r$

612 = 0.67), consistent with the cooking OA from many previous studies (e.g., Sun et al.,  
613 2011b; Ge et al., 2012a). All these results indicate the LOA may have significant  
614 contributions from cooking activities. However, the ratio of LOA/C<sub>6</sub>H<sub>10</sub>O<sup>+</sup> (622.0) in  
615 this study was much higher than that obtained in winter in Fresno and New York City  
616 (~180), and also its mass fraction to the total OA was a few times higher than previous  
617 results, suggesting that it contains species from other primary sources rather than only  
618 cooking emissions.

619 The LO-OOA MS profile exhibited characteristics of oxidized OA with enhanced  
620 signals at *m/z* 29 (CHO<sup>+</sup>), *m/z* 43 (mainly C<sub>2</sub>H<sub>3</sub>O<sup>+</sup>) and other oxygenated ions. Tight  
621 correlations between time series of LO-OOA and CHO<sup>+</sup> (*r* = 0.92), and C<sub>2</sub>H<sub>3</sub>O<sup>+</sup> (*r* = 0.73)  
622 were also observed. Moreover, we also noticed relatively high signals of the BBOA  
623 tracer ions C<sub>2</sub>H<sub>4</sub>O<sub>2</sub><sup>+</sup> and C<sub>3</sub>H<sub>5</sub>O<sub>2</sub><sup>+</sup> in the LO-OOA MS, and found good correlations  
624 between LO-OOA and BBOA tracers (*r* = 0.87 with C<sub>2</sub>H<sub>4</sub>O<sub>2</sub><sup>+</sup>, and *r* = 0.93 with  
625 C<sub>3</sub>H<sub>5</sub>O<sub>2</sub><sup>+</sup>), indicating possible influence from biomass burning. Thus, we compared mass  
626 fraction of LO-OOA to total OA in different seasons assuming that LO-OOA  
627 contributions would increase in straw-burning seasons given that it could be influenced  
628 by BBOA. Figure S6 showed the mass fraction of four factors during straw-burning  
629 seasons (spring, summer) and non-straw burning seasons (fall, winter). No obvious  
630 difference for LO-OOA fraction was found. Furthermore, the O/C and OM/OC ratios  
631 were 0.53 and 1.95, corresponding to 0.34 and 1.62 if calculated by using method of  
632 Aiken et al. (2008), well within the O/C range of less-oxidized OA factors identified in  
633 other studies (Jimenez et al., 2009), but beyond the O/C range of typical BBOA (0.18 -  
634 0.26) (He et al., 2010).

635 The MO-OOA factor had prominent peaks at *m/z* 28 (mainly CO<sup>+</sup>) and *m/z* 44  
636 (mainly CO<sub>2</sub><sup>+</sup>), and was dominated by C<sub>x</sub>H<sub>y</sub>O<sub>1</sub><sup>+</sup> (36.6%) and C<sub>x</sub>H<sub>y</sub>O<sub>2</sub><sup>+</sup> ions (29.0%) (Fig.  
637 10a). As a result, MO-OOA had a very high O/C ratio of 1.20, showing that it is heavily  
638 aged and processed OA component. Correspondingly, its time series correlated well with  
639 the secondary OA tracer ions, such as CO<sub>2</sub><sup>+</sup> (*r* = 0.93), C<sub>2</sub>H<sub>4</sub>O<sup>+</sup> (*r* = 0.67) and C<sub>2</sub>H<sub>3</sub>O<sup>+</sup> (*r*  
640 = 0.73) (Fig. 10b), etc.

641 The  $f_{44}$  (mass fraction of  $m/z$  44 to the total OA) vs.  $f_{43}$  (mass fraction of  $m/z$  43 to  
642 the total OA, defined by Ng et al. (2010)), can be used to investigate the degree of  
643 oxygenation of the identified factors. As presented in Fig. 11a, apart from NHOA, other  
644 three factors (LOA, LO-OOA and MO-OOA) all fall within the triangular region.  
645 MO-OOA located at the upper position with a higher  $f_{44}$  of 0.28, while LO-OOA  
646 located at the lower position of plot as it had a high fraction of  $f_{43}$  (0.09). This  
647 distribution of the four factors is also consistent with other studies.

648 The mass contributions of the four factors to total WSOA over the whole year are  
649 23.9% for NHOA, 31.2% for LOA, 15.3% for LO-OOA and 29.7% for MO-OOA (Fig.  
650 11b). POA (= NHOA + LOA) overweighed SOA (= LO-OOA + MO-OOA) mass,  
651 showing the dominant role of local anthropogenic emissions to the aerosol pollution in  
652 Changzhou, similar to that observed in Nanjing (Wang et al., 2016b). However, during  
653 spring and winter, SOA contributions dominate over POA, indicating significant SOA  
654 formation in particular the MO-OOA during cold seasons, which is in agreement with  
655 the OC/EC results.

656

### 657 **3.7 Back trajectory clustering analysis**

658 The Hybrid Single-particle Lagrangian Intergrated trajectory (HYSPLIT) model  
659 (Draxler et al., 2012) was used to investigate the origins of air masses based on the  
660 meteorological data available at the National Oceanic and Atmospheric Administration  
661 (NOAA) Global Data Assimilation System (GDAS). The 72h back trajectories of air  
662 parcels at 100 m above ground level in Changzhou were calculated at 8:00 local time  
663 (LT) throughout the campaign, and the results were presented in Fig. 12. The 4-, 5-, 4-,  
664 and 4-cluster solutions were adopted for spring, summer, fall and winter, respectively.  
665 During summer, air masses from southeast, east and west directions, passing over  
666 Shanghai and Anhui province, dominated the trajectories (75%) air masses. West and  
667 northwest air parcels dominated during winter, which may intercept air pollutants from  
668 Hebei and Anhui province. Considering the relatively short sampling days in each  
669 season, a more detailed discussion that is useful to distinguish contributions of local,  
670 regional and long-range transport to the air pollution, will be the subject of our future

671 work.

672

#### 673 **4. Conclusions**

674 We presented here the comprehensive characterization results on the PM<sub>2.5</sub> samples  
675 collected across one year in Changzhou City, located in the YRD region of China. The  
676 species we quantified including WSIs, trace metals, EC, WSOA, WIOA and also PAHs,  
677 can reproduce on average ~80% mass of the PM<sub>2.5</sub> (108.3 μg m<sup>-3</sup>). WSIs were the major  
678 component, accounting for 52.1% PM<sub>2.5</sub> mass, and NO<sub>3</sub><sup>-</sup>, SO<sub>4</sub><sup>2-</sup>, NH<sub>4</sub><sup>+</sup> were three most  
679 abundant ions. The organic matter (the sum of WSOA and WIOA) occupied 21.5%  
680 PM<sub>2.5</sub> mass, and EC accounted for ~5% PM<sub>2.5</sub> mass. Trace metal elements accounted for  
681 ~5% and ~2.7% PM<sub>2.5</sub> mass during winter and spring. Total PAHs concentrations were  
682 found to be at a relatively high concentration of 140.25 ng m<sup>-3</sup> in winter, above three  
683 times the average mass loading of 41.42 ng m<sup>-3</sup> in spring, both with InP, BghiP and Chr  
684 as the three most abundant PAHs. Average mass ratio of NO<sub>3</sub><sup>-</sup>/SO<sub>4</sub><sup>2-</sup> was 1.21,  
685 suggesting a significant role of traffic emissions, which is in consistent with the source  
686 analyses results based on the diagnostic ratios of the selected PAHs (BaP/BghiP,  
687 Flua/(Flua+Pyr) and BaP/(BaP+Chr)). In addition, a high Cl<sup>-</sup>/Na<sup>+</sup> ratio and the  
688 diagnostic ratio of Phe/(Ant+Phe) indicated also the contribution from coal combustion,  
689 in particular during winter.

690 In order to obtain further information regarding particle source, we analyzed the  
691 WSOA using SP-AMS and conducted PMF analyses on the HRMS of WSOA. Four OA  
692 factors including NHOA, LOA, LO-OOA and MO-OOA were identified. The mean  
693 mass contribution of POA was larger than that of SOA, revealing that local  
694 anthropogenic activities are the major drivers of PM pollution in Changzhou.  
695 Nevertheless, during cold seasons, SOA mass contribution increased, indicating  
696 significant role of secondarily formed species as well, thus reduction of air pollution in  
697 Changzhou should be paid on the strict emission control of both primary particles and  
698 the gaseous secondary aerosol precursors. One interesting finding in this work is the  
699 enrichment of organic nitrogen species in WSOA, and source analysis indicates that



700 traffic emissions can be a significant contributor to these species, which warrants more  
701 detailed investigations in the future. Also, more offline samples should be collected to  
702 achieve a more robust PMF analyses. Simultaneous online AMS measurement on the  
703 fine particles and measurements of gaseous species (SO<sub>2</sub>, NO<sub>2</sub>, O<sub>3</sub>, CO and some  
704 volatile organic compounds) are also essential to better understand the aerosol  
705 characteristics, and to implement proper measures to abate the air pollution in this  
706 region.

707

### 708 **Acknowledgements**

709 This work was supported the Natural Science Foundation of China (Grant Nos.  
710 (21407079 and 91544220), the Jiangsu National Science Foundation (BK20150042), the  
711 Specially-Appointed Professors Foundation and Jiangsu Innovation and  
712 Entrepreneurship Program (for X.G.), and the Major Research Development Program of  
713 Jiangsu Province (BE2016657 and BY2016030-15). We would also like to acknowledge  
714 Mr. Gang Li from Chinese academy of Science for providing us the OC/EC  
715 measurements.

716

### 717 **References:**

718 Aiken, A. C., Decarlo, P. F., Kroll, J. H., Worsnop, D. R., Huffman, J. A., Docherty, K. S.,  
719 Ulbrich, I. M., Mohr, C., Kimmel, J. R., Sueper, D., Sun, Y., Zhang, Q., Trimborn, A.,  
720 Northway, M., Ziemann, P. J., Canagaratna, M. R., Onasch, T. B., Alfarra, M. R., Prevot, A. S.  
721 H., Dommen, J., Duplissy, J., Metzger, A., Baltensperger, U., and Jimenez, J. L.: O/C and  
722 OM/OC ratios of primary, secondary, and ambient organic aerosols with high-resolution  
723 time-of-flight aerosol mass spectrometry, *Environ. Sci. Technol.*, 42, 4478-4485, doi:  
724 10.1021/Es703009q, 2008.

725 Anderson, J. O., Thundiyil, J. G., and Stolbach, A.: Clearing the air: A review of the effects of  
726 particulate matter air pollution on human health, *J. Med. Toxicol.*, 8, 166-175, doi:  
727 10.1007/s13181-011-0203-1, 2012.

728 Arimoto, R., Duce, R. A., Savoie, D. L., Prospero, J. M., Talbot, R., Cullen, J. D., Tomza, U.,  
729 Lewis, N. F., and Ray, B. J.: Relationships among aerosol constituents from Asia and the North  
730 Pacific during PEM-West A, *J. Geophys. Res. -Atmos.*, 101, 2011-2023, doi:  
731 10.1029/95JD01071, 1996.

732 Bozzetti, C., Sosedova, Y., Xiao, M., Daellenbach, K. R., Ulevicius, V., Dudoitis, V., Mordas,

733 G., Byčenkienė, S., Plauškaitė, K., Vlachou, A., Golly, B., Chazeau, B., Besombes, J. L.,  
734 Baltensperger, U., Jaffrezo, J. L., Slowik, J. G., El Haddad, I., and Prévôt, A. S. H.: Argon  
735 offline-AMS source apportionment of organic aerosol over yearly cycles for an urban, rural, and  
736 marine site in northern Europe, *Atmos. Chem. Phys.*, 17, 117-141, doi:  
737 10.5194/acp-17-117-2017, 2017.

738 Canagaratna, M. R., Jayne, J. T., Jimenez, J. L., Allan, J. D., Alfarra, M. R., Zhang, Q., Onasch,  
739 T. B., Drewnick, F., Coe, H., Middlebrook, A., Delia, A., Williams, L. R., Trimborn, A. M.,  
740 Northway, M. J., DeCarlo, P. F., Kolb, C. E., Davidovits, P., and Worsnop, D. R.: Chemical and  
741 microphysical characterization of ambient aerosols with the aerodyne aerosol mass spectrometer,  
742 *Mass Spectrom Rev*, 26, 185-222, doi: 10.1002/Mas.20115, 2007.

743 Canagaratna, M. R., Jimenez, J. L., Kroll, J. H., Chen, Q., Kessler, S. H., Massoli, P.,  
744 Hildebrandt Ruiz, L., Fortner, E., Williams, L. R., Wilson, K. R., Surratt, J. D., Donahue, N. M.,  
745 Jayne, J. T., and Worsnop, D. R.: Elemental ratio measurements of organic compounds using  
746 aerosol mass spectrometry: characterization, improved calibration, and implications, *Atmos.*  
747 *Chem. Phys.*, 15, 253-272, doi: 10.5194/acp-15-253-2015, 2015.

748 Cao, J. J., Xu, H. M., Xu, Q., Chen, B. H., and Kan, H. D.: Fine particulate matter constituents  
749 and cardiopulmonary mortality in a heavily polluted Chinese city, *Environ. Health Persp.*, 120,  
750 373-378, doi: 10.1289/ehp.1103671, 2012.

751 Cheng, Y., He, K. B., Du, Z. Y., Zheng, M., Duan, F. K., and Ma, Y. L.: Humidity plays an  
752 important role in the PM<sub>2.5</sub> pollution in Beijing, *Environ. Pollut.*, 197, 68-75, doi:  
753 10.1016/j.envpol.2014.11.028, 2015.

754 Chow, J. C., Watson, J. G., Chen, L. W. A., Arnott, W. P., Moosmüller, H., and Fung, K.:  
755 Equivalence of elemental carbon by thermal/optical reflectance and transmittance with different  
756 temperature protocols, *Environ. Sci. Technol.*, 38, 4414-4422, doi: 10.1021/es034936u, 2004.

757 Chow, J. C., Watson, J. G., Louie, P. K., Chen, L. W., and Sin, D.: Comparison of PM<sub>2.5</sub> carbon  
758 measurement methods in Hong Kong, China, *Environ. Pollut.*, 137, 334-344, doi:  
759 10.1016/j.envpol.2005.01.006, 2005.

760 Daellenbach, K. R., Bozzetti, C., Křepelová, A., Canonaco, F., Wolf, R., Zotter, P., Fermo, P.,  
761 Crippa, M., Slowik, J. G., Sosedova, Y., Zhang, Y., Huang, R. J., Poulain, L., Szidat, S.,  
762 Baltensperger, U., El Haddad, I., and Prévôt, A. S. H.: Characterization and source  
763 apportionment of organic aerosol using offline aerosol mass spectrometry, *Atmos. Meas. Tech.*,  
764 9, 23-39, doi: 10.5194/amt-9-23-2016, 2016.

765 Ding, A. J., Fu, C. B., Yang, X. Q., Sun, J. N., Zheng, L. F., Xie, Y. N., Herrmann, E., Nie, W.,  
766 Petaja, T., Kerminen, V. M., and Kulmala, M.: Ozone and fine particle in the western Yangtze  
767 River Delta: an overview of 1 yr data at the SORPES station, *Atmos. Chem. Phys.*, 13,  
768 5813-5830, doi: 10.5194/acp-13-5813-2013, 2013.

769 Draxler, R., Stunder, B., Rolph, G., Stein, A., and Taylor, A.: HYSPLIT4 user's guide, version 4,

- 770 report, NOAA, Silver Spring, MD, doi, 2012.
- 771 Drewnick, F.: Speciation analysis in on-line aerosol mass spectrometry, *Anal. Bioanal. Chem.*,  
772 404, 2127-2131, doi: 10.1007/s00216-012-6295-x, 2012.
- 773 Duan, F., Liu, X., He, K., and Dong, S.: Measurements and characteristics of  
774 nitrogen-containing compounds in atmospheric particulate matter in Beijing, China, *Bull.*  
775 *Environ. Contam. Toxicol.*, 82, 332-337, doi: 10.1007/s00128-008-9560-0, 2009.
- 776 Duan, J., Tan, J., Wang, S., Chai, F., He, K., and Hao, J.: Roadside, urban, and rural comparison  
777 of size distribution characteristics of PAHs and carbonaceous components of Beijing, China, *J.*  
778 *Atmos. Chem.*, 69, 337-349, doi: 10.1007/s10874-012-9242-5, 2012.
- 779 Dzepina, K., Arey, J., Marr, L. C., Worsnop, D. R., Salcedo, D., Zhang, Q., Onasch, T. B.,  
780 Molina, L. T., Molina, M. J., and Jimenez, J. L.: Detection of particle-phase polycyclic aromatic  
781 hydrocarbons in Mexico City using an aerosol mass spectrometer, *Int. J. Mass Spectrom.*, 263,  
782 152-170, doi: 10.1016/j.ijms.2007.01.010, 2007.
- 783 Fan, J., Yue, X., Jing, Y., Chen, Q., and Wang, S.: Online monitoring of water-soluble ionic  
784 composition of PM10 during early summer over Lanzhou City, *J. Environ. Sci.*, 26, 353-361, doi:  
785 10.1016/s1001-0742(13)60431-3, 2014.
- 786 Feng, J., Hu, J., Xu, B., Hu, X., Sun, P., Han, W., Gu, Z., Yu, X., and Wu, M.: Characteristics  
787 and seasonal variation of organic matter in PM2.5 at a regional background site of the Yangtze  
788 River Delta region, China, *Atmos. Environ.*, 123, 288-297, doi: 10.1016/j.atmosenv.2015.08.019,  
789 2015.
- 790 Feng, Y., Chen, Y., Guo, H., Zhi, G., Xiong, S., Li, J., Sheng, G., and Fu, J.: Characteristics of  
791 organic and elemental carbon in PM2.5 samples in Shanghai, China, *Atmos. Res.*, 92, 434-442,  
792 doi: 10.1016/j.atmosres.2009.01.003, 2009.
- 793 Fu, H., Zhang, M., Li, W., Chen, J., Wang, L., Quan, X., and Wang, W.: Morphology,  
794 composition and mixing state of individual carbonaceous aerosol in urban Shanghai, *Atmos.*  
795 *Chem. Phys.*, 12, 693-707, doi: 10.5194/acp-12-693-2012, 2012.
- 796 Ge, X., Wexler, A. S., and Clegg, S. L.: Atmospheric amines - Part II. Thermodynamic  
797 properties and gas/particle partitioning, *Atmos. Environ.*, 45, 561-577, doi: DOI  
798 10.1016/j.atmosenv.2010.10.013, 2011a.
- 799 Ge, X., Wexler, A. S., and Clegg, S. L.: Atmospheric amines - Part I. A review, *Atmos. Environ.*,  
800 45, 524-546, doi: DOI 10.1016/j.atmosenv.2010.10.012, 2011b.
- 801 Ge, X., Setyan, A., Sun, Y., and Zhang, Q.: Primary and secondary organic aerosols in Fresno,  
802 California during wintertime: Results from high resolution aerosol mass spectrometry, *J.*  
803 *Geophys. Res. -Atmos.*, 117, D19301, doi: 10.1029/2012jd018026, 2012a.
- 804 Ge, X., Zhang, Q., Sun, Y., Ruehl, C. R., and Setyan, A.: Effect of aqueous-phase processing on

805 aerosol chemistry and size distributions in Fresno, California, during wintertime, *Environ.*  
806 *Chem.*, 9, 221-235, doi: 10.1071/EN11168, 2012b.

807 Ge, X., Shaw, S. L., and Zhang, Q.: Toward understanding amines and their degradation  
808 products from postcombustion CO<sub>2</sub> capture processes with aerosol mass spectrometry, *Environ.*  
809 *Sci. Technol.*, 48, 5066-5075, doi: 10.1021/es4056966, 2014.

810 Ge, X., Wang, J., Zhang, Z., Wang, X., and Chen, M.: Thermodynamic modeling of electrolyte  
811 solutions by a hybrid ion-interaction and solvation (HIS) model, *Calphad*, 48, 79-88, doi:  
812 10.1016/j.calphad.2014.11.001, 2015.

813 Gu, J., Bai, Z., Liu, A., Wu, L., Xie, Y., Li, W., Dong, H., and Zhang, X.: Characterization of  
814 atmospheric organic carbon and element carbon of PM<sub>2.5</sub> and PM<sub>10</sub> at Tianjin, China, *Aerosol*  
815 *Air Qual. Res.*, 10, 167-176, doi: 10.4209/aaqr.2009.12.0080, 2010.

816 Gu, J., Du, S., Han, D., Hou, L., Yi, J., Xu, J., Liu, G., Han, B., Yang, G., and Bai, Z.-P.: Major  
817 chemical compositions, possible sources, and mass closure analysis of PM<sub>2.5</sub> in Jinan, China,  
818 *Air Qual. Atmos. Health*, 7, 251-262, doi: 10.1007/s11869-013-0232-9, 2014.

819 He, J., Fan, S., Meng, Q., Sun, Y., Zhang, J., and Zu, F.: Polycyclic aromatic hydrocarbons  
820 (PAHs) associated with fine particulate matters in Nanjing, China: Distributions, sources and  
821 meteorological influences, *Atmos. Environ.*, 89, 207-215, doi: 10.1016/j.atmosenv.2014.02.042,  
822 2014.

823 He, L. Y., Lin, Y., Huang, X. F., Guo, S., Xue, L., Su, Q., Hu, M., Luan, S. J., and Zhang, Y. H.:  
824 Characterization of high-resolution aerosol mass spectra of primary organic aerosol emissions  
825 from Chinese cooking and biomass burning, *Atmos. Chem. Phys.*, 10, 11535-11543, doi:  
826 10.5194/acp-10-11535-2010, 2010.

827 Heal, M. R., Kumar, P., and Harrison, R. M.: Particles, air quality, policy and health, *Chem. Soc.*  
828 *Rev.*, doi, 2012.

829 Ho, K. F., Ho, S. S. H., Huang, R.-J., Liu, S. X., Cao, J.-J., Zhang, T., Chuang, H.-C., Chan, C.  
830 S., Hu, D., and Tian, L.: Characteristics of water-soluble organic nitrogen in fine particulate  
831 matter in the continental area of China, *Atmos. Environ.*, 106, 252-261, doi:  
832 10.1016/j.atmosenv.2015.02.010, 2015.

833 Hu, J., Ying, Q., Wang, Y., and Zhang, H.: Characterizing multi-pollutant air pollution in China:  
834 Comparison of three air quality indices, *Environ. Int.*, 84, 17-25, doi:  
835 10.1016/j.envint.2015.06.014, 2015.

836 Hu, W., Hu, M., Hu, W., Jimenez, J. L., Yuan, B., Chen, W., Wang, M., Wu, Y., Chen, C.,  
837 Wang, Z., Peng, J., Zeng, L., and Shao, M.: Chemical composition, sources, and aging process  
838 of submicron aerosols in Beijing: Contrast between summer and winter, *J. Geophys. Res.*  
839 *-Atmos.*, 121, 2015JD024020, doi: 10.1002/2015JD024020, 2016.

840 Hu, X., Zhang, Y., Ding, Z., Wang, T., Lian, H., Sun, Y., and Wu, J.: Bioaccessibility and health

841 risk of arsenic and heavy metals (Cd, Co, Cr, Cu, Ni, Pb, Zn and Mn) in TSP and PM<sub>2.5</sub> in  
842 Nanjing, China, *Atmos. Environ.*, 57, 146-152, doi: 10.1016/j.atmosenv.2012.04.056, 2012.

843 Huang, R., Zhang, Y., Bozzetti, C., Ho, K., Cao, J., Han, Y., Daellenbach, K. R., Slowik, J. G.,  
844 Platt, S. M., Canonaco, F., Zotter, P., Wolf, R., Pieber, S. M., Bruns, E. A., Crippa, M., Ciarelli,  
845 G., Piazzalunga, A., Schwikowski, M., Abbaszade, G., Schnelle-Kreis, J., Zimmermann, R., An,  
846 Z., Szidat, S., Baltensperger, U., Haddad, I. E., and Prevot, A. S. H.: High secondary aerosol  
847 contribution to particulate pollution during haze events in China, *Nature*, 514, 218-222, doi:  
848 10.1038/nature13774, 2014.

849 Huang, T., Chen, J., Zhao, W., Cheng, J., and Cheng, S.: Seasonal variations and correlation  
850 analysis of water-soluble inorganic ions in PM<sub>2.5</sub> in Wuhan, 2013, *Atmosphere*, 7, 49, doi:  
851 10.3390/atmos7040049, 2016.

852 Huang, X. F., He, L. Y., Hu, M., Canagaratna, M. R., Sun, Y., Zhang, Q., Zhu, T., Xue, L., Zeng,  
853 L. W., Liu, X. G., Zhang, Y. H., Jayne, J. T., Ng, N. L., and Worsnop, D. R.: Highly  
854 time-resolved chemical characterization of atmospheric submicron particles during 2008 Beijing  
855 Olympic Games using an Aerodyne High-Resolution Aerosol Mass Spectrometer, *Atmos. Chem.*  
856 *Phys.*, 10, 8933-8945, doi: 10.5194/acp-10-8933-2010, 2010.

857 Jimenez, J. L., Canagaratna, M. R., Donahue, N. M., Prevot, A. S. H., Zhang, Q., Kroll, J. H.,  
858 DeCarlo, P. F., Allan, J. D., Coe, H., Ng, N. L., Aiken, A. C., Docherty, K. S., Ulbrich, I. M.,  
859 Grieshop, A. P., Robinson, A. L., Duplissy, J., Smith, J. D., Wilson, K. R., Lanz, V. A., Hueglin,  
860 C., Sun, Y. L., Tian, J., Laaksonen, A., Raatikainen, T., Rautiainen, J., Vaattovaara, P., Ehn, M.,  
861 Kulmala, M., Tomlinson, J. M., Collins, D. R., Cubison, M. J., Dunlea, E. J., Huffman, J. A.,  
862 Onasch, T. B., Alfarra, M. R., Williams, P. I., Bower, K., Kondo, Y., Schneider, J., Drewnick, F.,  
863 Borrmann, S., Weimer, S., Demerjian, K., Salcedo, D., Cottrell, L., Griffin, R., Takami, A.,  
864 Miyoshi, T., Hatakeyama, S., Shimono, A., Sun, J. Y., Zhang, Y. M., Dzepina, K., Kimmel, J. R.,  
865 Sueper, D., Jayne, J. T., Herndon, S. C., Trimborn, A. M., Williams, L. R., Wood, E. C.,  
866 Middlebrook, A. M., Kolb, C. E., Baltensperger, U., and Worsnop, D. R.: Evolution of organic  
867 aerosols in the atmosphere, *Science*, 326, 1525-1529, doi: 10.1126/science.1180353, 2009.

868 Khalili, N. R., Scheff, P. A., and Holsen, T. M.: PAH source fingerprints for coke ovens, diesel  
869 and, gasoline engines, highway tunnels, and wood combustion emissions, *Atmos. Environ.*, 29,  
870 533-542, doi: 10.1016/1352-2310(94)00275-P, 1995.

871 Kong, S., Ding, X., Bai, Z., Han, B., Chen, L., Shi, J., and Li, Z.: A seasonal study of polycyclic  
872 aromatic hydrocarbons in PM(2.5) and PM(2.5-10) in five typical cities of Liaoning Province,  
873 China, *J. Hazard. Mater.*, 183, 70-80, doi: 10.1016/j.jhazmat.2010.06.107, 2010.

874 Kong, S., Li, X., Li, L., Yin, Y., Chen, K., Yuan, L., Zhang, Y., Shan, Y., and Ji, Y.: Variation  
875 of polycyclic aromatic hydrocarbons in atmospheric PM<sub>2.5</sub> during winter haze period around  
876 2014 Chinese Spring Festival at Nanjing: Insights of source changes, air mass direction and  
877 firework particle injection, *Sci. Total Environ.*, 520, 59-72, doi: 10.1016/j.scitotenv.2015.03.001,  
878 2015.

879 Kulmala, M., Lappalainen, H. K., Petäjä, T., Kurten, T., Kerminen, V. M., Viisanen, Y., Hari, P.,  
880 Sorvari, S., Bäck, J., Bondur, V., Kasimov, N., Kotlyakov, V., Matvienko, G., Baklanov, A.,  
881 Guo, H. D., Ding, A., Hansson, H. C., and Zilitinkevich, S.: Introduction: The Pan-Eurasian  
882 Experiment (PEEX) – multidisciplinary, multiscale and multicomponent research and  
883 capacity-building initiative, *Atmos. Chem. Phys.*, 15, 13085-13096, doi:  
884 10.5194/acp-15-13085-2015, 2015.

885 Lee, A. K. Y., Willis, M. D., Healy, R. M., Onasch, T. B., and Abbatt, J. P. D.: Mixing state of  
886 carbonaceous aerosol in an urban environment: single particle characterization using the soot  
887 particle aerosol mass spectrometer (SP-AMS), *Atmos. Chem. Phys.*, 15, 1823-1841, doi:  
888 10.5194/acp-15-1823-2015, 2015.

889 Li, B., Zhang, J., Zhao, Y., Yuan, S., Zhao, Q., Shen, G., and Wu, H.: Seasonal variation of  
890 urban carbonaceous aerosols in a typical city Nanjing in Yangtze River Delta, China, *Atmos.*  
891 *Environ.*, 106, 223-231, doi: 10.1016/j.atmosenv.2015.01.064, 2015.

892 Liu, G., Li, J., Wu, D., and Xu, H.: Chemical composition and source apportionment of the  
893 ambient PM<sub>2.5</sub> in Hangzhou, China, *Particuology*, 18, 135-143, doi:  
894 10.1016/j.partic.2014.03.011, 2015.

895 Meng, C. C., Wang, L. T., Zhang, F. F., Wei, Z., Ma, S. M., Ma, X., and Yang, J.:  
896 Characteristics of concentrations and water-soluble inorganic ions in PM<sub>2.5</sub> in Handan City,  
897 Hebei province, China, *Atmos. Res.*, 171, 133-146, doi: 10.1016/j.atmosres.2015.12.013, 2016.

898 Mihara, T., and Mochida, M.: Characterization of Solvent-Extractable Organics in Urban  
899 Aerosols Based on Mass Spectrum Analysis and Hygroscopic Growth Measurement, *Environ.*  
900 *Sci. Technol.*, 45, 9168-9174, doi: 10.1021/es201271w, 2011.

901 Mirante, F., Salvador, P., Pio, C., Alves, C., Artiñano, B., Caseiro, A., and Revuelta, M. A.: Size  
902 fractionated aerosol composition at roadside and background environments in the Madrid urban  
903 atmosphere, *Atmos. Res.*, 138, 278-292, doi: 10.1016/j.atmosres.2013.11.024, 2014.

904 Ng, N. L., Canagaratna, M. R., Zhang, Q., Jimenez, J. L., Tian, J., Ulbrich, I. M., Kroll, J. H.,  
905 Docherty, K. S., Chhabra, P. S., Bahreini, R., Murphy, S. M., Seinfeld, J. H., Hildebrandt, L.,  
906 Donahue, N. M., DeCarlo, P. F., Lanz, V. A., Prévôt, A. S. H., Dinar, E., Rudich, Y., and  
907 Worsnop, D. R.: Organic aerosol components observed in Northern Hemispheric datasets from  
908 Aerosol Mass Spectrometry, *Atmos. Chem. Phys.*, 10, 4625-4641, doi:  
909 10.5194/acp-10-4625-2010, 2010.

910 Ng, N. L., Canagaratna, M. R., Jimenez, J. L., Zhang, Q., Ulbrich, I. M., and Worsnop, D. R.:  
911 Real-time methods for estimating organic component mass concentrations from aerosol mass  
912 spectrometer data, *Environ. Sci. Technol.*, 45, 910-916, doi: Doi 10.1021/Es102951k, 2011.

913 Onasch, T. B., Trimborn, A., Fortner, E. C., Jayne, J. T., Kok, G. L., Williams, L. R., Davidovits,  
914 P., and Worsnop, D. R.: Soot particle aerosol mass spectrometer: Development, validation, and  
915 initial application, *Aerosol Sci. Tech.*, 46, 804-817, doi: 10.1080/02786826.2012.663948, 2012.

916 Pan, Y., Tian, S., Liu, D., Fang, Y., Zhu, X., Zhang, Q., Zheng, B., Michalski, G., and Wang, Y.:  
917 Fossil Fuel Combustion-Related Emissions Dominate Atmospheric Ammonia Sources during  
918 Severe Haze Episodes: Evidence from  $^{15}\text{N}$ -Stable Isotope in Size-Resolved Aerosol  
919 Ammonium, *Environ. Sci. Technol.*, 50, 8049-8056, doi: 10.1021/acs.est.6b00634, 2016.

920 Qi, L., Chen, M., Ge, X., Zhang, Y., and Guo, B.: Seasonal variations and sources of 17 aerosol  
921 metal elements in suburban Nanjing, China, *Atmosphere*, 7, 153, doi, 2016a.

922 Qi, L., Zhang, Y., Ma, Y., Chen, M., Ge, X., Ma, Y., Zheng, J., Wang, Z., and Li, S.: Source  
923 identification of trace elements in the atmosphere during the second Asian Youth Games in  
924 Nanjing, China: Influence of control measures on air quality, *Atmos. Pollut. Res.*, 7, 547-556,  
925 doi: 10.1016/j.apr.2016.01.003, 2016b.

926 Qiao, T., Zhao, M., Xiu, G., and Yu, J.: Seasonal variations of water soluble composition  
927 (WSOC, Hulis and WSIs) in PM<sub>1</sub> and its implications on haze pollution in urban Shanghai,  
928 China, *Atmos. Environ.*, 123, 306-314, doi: 10.1016/j.atmosenv.2015.03.010, 2015.

929 Saldarriaga-Noreña, H., López-Márquez, R., Murillo-Tovar, M., Hernández-Mena, L.,  
930 Ospina-Noreña, E., Sánchez-Salinas, E., Waliszewski, S., and Montiel-Palma, S.: Analysis of  
931 PAHs associated with particulate matter PM<sub>2.5</sub> in two places at the city of Cuernavaca, Morelos,  
932 México, *Atmosphere*, 6, 1259-1270, doi: 10.3390/atmos6091259, 2015.

933 Shen, G. F., Yuan, S. Y., Xie, Y. N., Xia, S. J., Li, L., Yao, Y. K., Qiao, Y. Z., Zhang, J., Zhao,  
934 Q. Y., Ding, A. J., Li, B., and Wu, H. S.: Ambient levels and temporal variations of PM<sub>2.5</sub> and  
935 PM<sub>10</sub> at a residential site in the mega-city, Nanjing, in the western Yangtze River Delta, China,  
936 *J. Environ. Sci. Health A: Tox. Hazard. Subst. Environ.Eng.*, 49, 171-178, doi:  
937 10.1080/10934529.2013.838851, 2014.

938 Shi, J., Gao, H., Qi, J., Zhang, J., and Yao, X.: Sources, compositions, and distributions of  
939 water-soluble organic nitrogen in aerosols over the China Sea, *J. Geophys. Res. -Atmos.*, 115,  
940 doi: 10.1029/2009jd013238, 2010.

941 Sun, Y., Zhang, Q., Zheng, M., Ding, X., Edgerton, E. S., and Wang, X.: Characterization and  
942 source apportionment of water-soluble organic matter in atmospheric fine particles (PM<sub>2.5</sub>) with  
943 high-resolution aerosol mass spectrometry and GC-MS, *Environ. Sci. Technol.*, 45, 4854-4861,  
944 doi: 10.1021/es200162h, 2011a.

945 Sun, Y., Jiang, Q., Wang, Z., Fu, P., Li, J., Yang, T., and Yin, Y.: Investigation of the sources  
946 and evolution processes of severe haze pollution in Beijing in January 2013, *J. Geophys. Res.*  
947 *-Atmos.*, 119, 4380-4398, doi: 10.1002/2014jd021641, 2014.

948 Sun, Y., Du, W., Fu, P., Wang, Q., Li, J., Ge, X., Zhang, Q., Zhu, C., Ren, L., Xu, W., Zhao, J.,  
949 Han, T., Worsnop, D. R., and Wang, Z.: Primary and secondary aerosols in Beijing in winter:  
950 sources, variations and processes, *Atmos. Chem. Phys.*, 16, 8309-8329, doi:  
951 10.5194/acp-16-8309-2016, 2016.

952 Sun, Y. L., Zhang, Q., Schwab, J. J., Demerjian, K. L., Chen, W. N., Bae, M. S., Hung, H. M.,  
953 Hogrefe, O., Frank, B., Rattigan, O. V., and Lin, Y. C.: Characterization of the sources and  
954 processes of organic and inorganic aerosols in New York city with a high-resolution  
955 time-of-flight aerosol mass spectrometer, *Atmos. Chem. Phys.*, 11, 1581-1602, doi:  
956 10.5194/acp-11-1581-2011, 2011b.

957 Szabó, J., Nagy, A. S., and Erdős, J.: Ambient concentrations of PM<sub>10</sub>, PM<sub>10</sub>-bound polycyclic  
958 aromatic hydrocarbons and heavy metals in an urban site of Győr, Hungary, *Air Qual. Atmos.*  
959 *Health*, 8, 229-241, doi: 10.1007/s11869-015-0318-7, 2015.

960 Ulbrich, I. M., Canagaratna, M. R., Zhang, Q., Worsnop, D. R., and Jimenez, J. L.:  
961 Interpretation of organic components from Positive Matrix Factorization of aerosol mass  
962 spectrometric data, *Atmos. Chem. Phys.*, 9, 2891-2918, doi: 10.5194/acp-9-2891-2009, 2009.

963 Violaki, K., and Mihalopoulos, N.: Water-soluble organic nitrogen (WSON) in size-segregated  
964 atmospheric particles over the Eastern Mediterranean, *Atmos. Environ.*, 44, 4339-4345 doi,  
965 2010.

966 Wang, F., Lin, T., Feng, J., Fu, H., and Guo, Z.: Source apportionment of polycyclic aromatic  
967 hydrocarbons in PM<sub>2.5</sub> using positive matrix factorization modeling in Shanghai, China,  
968 *Environ. Sci. Process Impacts*, 17, 197-205, doi: 10.1039/c4em00570h, 2015.

969 Wang, F., Guo, Z., Lin, T., and Rose, N. L.: Seasonal variation of carbonaceous pollutants in  
970 PM<sub>2.5</sub> at an urban 'supersite' in Shanghai, China, *Chemosphere*, 146, 238-244, doi:  
971 10.1016/j.chemosphere.2015.12.036, 2016a.

972 Wang, G., Kawamura, K., Lee, S., Ho, K., and Cao, J.: Molecular, seasonal, and spatial  
973 distributions of organic aerosols from fourteen Chinese cities, *Environ. Sci. Technol.*, 40,  
974 4619-4625, doi: 10.1021/es060291x, 2006a.

975 Wang, J., Geng, N. B., Xu, Y. F., Zhang, W. D., Tang, X. Y., and Zhang, R. Q.: PAHs in PM<sub>2.5</sub>  
976 in Zhengzhou: concentration, carcinogenic risk analysis, and source apportionment, *Environ.*  
977 *Monit. Assess.*, 186, 7461-7473, doi: 10.1007/s10661-014-3940-1, 2014.

978 Wang, J., Ge, X., Chen, Y., Shen, Y., Zhang, Q., Sun, Y., Xu, J., Ge, S., Yu, H., and Chen, M.:  
979 Highly time-resolved urban aerosol characteristics during springtime in Yangtze River Delta,  
980 China: insights from soot particle aerosol mass spectrometry, *Atmos. Chem. Phys.*, 16,  
981 9109-9127, doi: 10.5194/acp-16-9109-2016, 2016b.

982 Wang, J., Onasch, T. B., Ge, X., Collier, S., Zhang, Q., Sun, Y., Yu, H., Chen, M., Prévôt, A. S.  
983 H., and Worsnop, D. R.: Observation of fullerene foot in eastern China, *Environ. Sci. Technol.*  
984 *Lett.*, 3, 121-126, doi: 10.1021/acs.estlett.6b00044, 2016c.

985 Wang, T., Jiang, F., Deng, J., Shen, Y., Fu, Q., Wang, Q., Fu, Y., Xu, J., and Zhang, D.: Urban  
986 air quality and regional haze weather forecast for Yangtze River Delta region, *Atmos. Environ.*,  
987 58, 70-83, doi: 10.1016/j.atmosenv.2012.01.014, 2012.



- 988 Wang, Y., Zhuang, G., Zhang, X., Huang, K., Xu, C., Tang, A., Chen, J., and An, Z.: The ion  
989 chemistry, seasonal cycle, and sources of PM<sub>2.5</sub> and TSP aerosol in Shanghai, *Atmos. Environ.*,  
990 40, 2935-2952, doi: 10.1016/j.atmosenv.2005.12.051, 2006b.
- 991 Xu, J., Zhang, Q., Li, X., Ge, X., Xiao, C., Ren, J., and Qin, D.: Dissolved organic matter and  
992 inorganic Ions in a central Himalayan glacier—Insights into chemical composition and  
993 atmospheric sources, *Environ. Sci. Technol.*, 47, 6181-6188, doi: 10.1021/es4009882, 2013.
- 994 Xu, J., Zhang, Q., Chen, M., Ge, X., Ren, J., and Qin, D.: Chemical composition, sources, and  
995 processes of urban aerosols during summertime in northwest China: insights from  
996 high-resolution aerosol mass spectrometry, *Atmos. Chem. Phys.*, 14, 12593-12611, doi:  
997 10.5194/acp-14-12593-2014, 2014.
- 998 Xu, J., Zhang, Q., Wang, Z., Yu, G., Ge, X., and Qin, X.: Chemical composition and size  
999 distribution of summertime PM<sub>2.5</sub> at a high altitude remote location in the northeast of the  
1000 Qinghai–Xizang (Tibet) Plateau: insights into aerosol sources and processing in free troposphere,  
1001 *Atmos. Chem. Phys.*, 15, 5069-5081, doi: 10.5194/acp-15-5069-2015, 2015.
- 1002 Xu, L., Guo, H., Weber, R. J., and Ng, N. L.: Chemical Characterization of Water-Soluble  
1003 Organic Aerosol in Contrasting Rural and Urban Environments in the Southeastern United  
1004 States, *Environ. Sci. Technol.*, 51, 78-88, doi: 10.1021/acs.est.6b05002, 2017.
- 1005 Ye, X. N., Ma, Z., Hu, D. W., Yang, X., and Chen, J. M.: Size-resolved hygroscopicity of  
1006 submicrometer urban aerosols in Shanghai during wintertime, *Atmos. Res.*, 99, 353-364, doi:  
1007 10.1016/j.atmosres.2010.11.008, 2011.
- 1008 Zhang, Q., Jimenez, J. L., Canagaratna, M. R., Allan, J. D., Coe, H., Ulbrich, I., Alfarra, M. R.,  
1009 Takami, A., Middlebrook, A. M., Sun, Y. L., Dzepina, K., Dunlea, E., Docherty, K., DeCarlo, P.  
1010 F., Salcedo, D., Onasch, T., Jayne, J. T., Miyoshi, T., Shimo, A., Hatakeyama, S., Takegawa,  
1011 N., Kondo, Y., Schneider, J., Drewnick, F., Borrmann, S., Weimer, S., Demerjian, K., Williams,  
1012 P., Bower, K., Bahreini, R., Cottrell, L., Griffin, R. J., Rautiainen, J., Sun, J. Y., Zhang, Y. M.,  
1013 and Worsnop, D. R.: Ubiquity and dominance of oxygenated species in organic aerosols in  
1014 anthropogenically-influenced Northern Hemisphere midlatitudes, *Geophys. Res. Lett.*, 34,  
1015 n/a-n/a, doi: 10.1029/2007gl029979, 2007a.
- 1016 Zhang, Q., Jimenez, J. L., Worsnop, D. R., and Canagaratna, M.: A case study of urban particle  
1017 acidity and its influence on secondary organic aerosol, *Environ. Sci. Technol.*, 41, 3213-3219,  
1018 doi: 10.1021/Es061812j, 2007b.
- 1019 Zhang, Q., Jimenez, J. L., Canagaratna, M. R., Ulbrich, I. M., Ng, N. L., Worsnop, D. R., and  
1020 Sun, Y.: Understanding atmospheric organic aerosols via factor analysis of aerosol mass  
1021 spectrometry: a review, *Anal. Bioanal. Chem.*, 401, 3045-3067, doi:  
1022 10.1007/s00216-011-5355-y, 2011.
- 1023 Zhang, R., Jing, J., Tao, J., Hsu, S. C., Wang, G., Cao, J., Lee, C. S. L., Zhu, L., Chen, Z., Zhao,  
1024 Y., and Shen, Z.: Chemical characterization and source apportionment of PM<sub>2.5</sub> in Beijing:

1025 seasonal perspective, *Atmos. Chem. Phys.*, 13, 7053-7074, doi: 10.5194/acp-13-7053-2013,  
1026 2013.

1027 Zhang, Y. J., Tang, L., Yu, H., Wang, Z., Sun, Y., Qin, W., Chen, W., Chen, C., Ding, A., Wu,  
1028 J., Ge, S., Chen, C., and Zhou, H.-c.: Chemical composition, sources and evolution processes of  
1029 aerosol at an urban site in Yangtze River Delta, China during wintertime, *Atmos. Environ.*, 123,  
1030 339-349, doi: 10.1016/j.atmosenv.2015.08.017, 2016.

1031 Zhao, M., Huang, Z., Qiao, T., Zhang, Y., Xiu, G., and Yu, J.: Chemical characterization, the  
1032 transport pathways and potential sources of PM<sub>2.5</sub> in Shanghai: Seasonal variations, *Atmos.*  
1033 *Res.*, 158-159, 66-78, doi: 10.1016/j.atmosres.2015.02.003, 2015.

1034 Zhou, J., Xing, Z., Deng, J., and Du, K.: Characterizing and sourcing ambient PM<sub>2.5</sub> over key  
1035 emission regions in China I: Water-soluble ions and carbonaceous fractions, *Atmos. Environ.*,  
1036 135, 20-30, doi: 10.1016/j.atmosenv.2016.03.054, 2016.  
1037  
1038

1039 Table 1. Average meteorological parameters during four seasons

Parameters	Spring	Summer	Fall	Winter
RH (%)	57.3±11.4	61.1±11.8	65.5±10.9	62.3±10.6
T(°C)	13.1±4.0	32.1±4.3	21.6±2.3	5.6±1.8
WS(m s <sup>-1</sup> )	1.1±0.4	1.6±0.6	0.9±0.4	0.9±0.3
WD <sup>a</sup>	SE	E,W,SE	E	W,NW,SE

1040 <sup>a</sup> Refer to prevailing wind directions, E—East, SE—Southeast, W—West,

1041 NW-Northwest.

1042

1043 Table 2. Summary of aerosol species, analytical methods, measurement uncertainties  
 1044 and the method detection limits (MDLs).

<b>Species</b>	<b>Analytical methods</b>	<b>Uncertainties</b>	<b>MDLs</b>
Water soluble ions	Ion chromatography	3.5 - 7.0%	3 - 20 $\mu\text{g L}^{-1}$
Trace elements	ICP-OES	10.3 - 18.5%	-
OC, EC	Thermal-Optical Carbon Analyzer	<12%	30 - 80 $\text{ng m}^{-3}$ for OC and 30 $\text{ng m}^{-3}$ for EC (Mirante et al., 2014)
WSOC	TOC analyzer	3.4 - 6.0%	5.0 $\mu\text{g L}^{-1}$
PAH	GC-MS	20%	2 - 5 $\mu\text{g L}^{-1}$
OM/OC ratio	SP-AMS	6% (Aiken et al., 2008)	-
WSOA	SP-AMS, TOC	6.9 - 8.5%	-

1045

1046 Table 3. Summary of the mean concentrations (with one standard deviation) and mass  
 1047 fractions for PM<sub>2.5</sub> and all quantified components in four seasons and the whole  
 1048 sampling period, respectively.

Species ( $\mu\text{g m}^{-3}$ )	Spring	Summer	Fall	Winter	Annual
<b>PM<sub>2.5</sub></b>	<b>106.0±24.4</b>	<b>80.9±37.7</b>	<b>103.3±28.2</b>	<b>126.9±50.4</b>	<b>108.3±40.8</b>
<b>WSIIs</b>	<b>66.5±17.2</b>	<b>35.0±20.2</b>	<b>51.0±17.2</b>	<b>66.8±23.6</b>	<b>56.4±22.9</b>
Sulfate	17.3±4.8	15.8±9.8	17.2±6.2	18.7±7.6	17.5±7.1
Nitrate	26.4±8.7	6.8±6.2	17.0±9.0	24.1±11.8	19.3±11.6
Ammonium	14.8±4.2	8.2±4.3	11.2±3.2	13.1±3.7	12.0±4.2
Other ions	8.0±2.3	4.2±2.9	5.6±1.5	10.9±3.4	7.6±3.7
% of PM <sub>2.5</sub>	62.7±4.9	43.2±7.4	49.3±8.5	52.6±7.3	52.1±9.7
<b>TC</b>	<b>16.0±3.3</b>	<b>12.1±1.6</b>	<b>21.0±11.8</b>	<b>22.3±8.6</b>	<b>19.2±9.3</b>
OC	11.2±2.6	7.9±0.8	13.2±7.8	18.3±8.1	13.8±7.5
EC	4.8±0.9	4.2±1.2	7.7±4.5	4.0±0.9	5.4±3.2
% of PM <sub>2.5</sub>	15.0±2.5	15.0±6.5	20.3±8.2	17.6±3.3	17.8±6.1
<b>OA</b>	<b>18.9±4.1</b>	<b>14.0±1.4</b>	<b>21.6±11.9</b>	<b>31.2±11.9</b>	<b>23.3±9.0</b>
WSOA	14.1±3.0	12.1±2.4	15.6±6.6	25.1±8.6	18.1±6.1
WIOA	4.8±2.6	1.9±1.8	5.9±7.2	6.1±10.6	5.2±7.6
% of PM <sub>2.5</sub>	17.8±3.2	18.2±8.4	20.9±8.3	24.6±6.3	21.5±6.8
<b>PAHs (<math>\text{ng m}^{-3}</math>)</b>	<b>41.42±24.7</b>			<b>140.25±60.2</b>	
<b>Trace elements</b>			<b>2.77±1.15</b>	<b>6.38±3.14</b>	
<b>OA+EC+WSIIs</b>	<b>90.2±21.0</b>	<b>53.2±21.6</b>	<b>83.1±29.6*</b>	<b>108.4±36.3*</b>	<b>85.1±27.9</b>
<b>% of PM<sub>2.5</sub></b>	<b>85.1±5.6</b>	<b>65.8±5.4</b>	<b>80.4±15.0*</b>	<b>85.4±12.9*</b>	<b>78.6±11.6</b>

1049 \*These values also include contributions from trace elements.

1050

1051

1052

1053

1054

1055

1056 Table 4. Mean concentration ( $\text{ng m}^{-3}$ ) and mass fractions (%) of individual PAH to the total  
 1057 PAHs.

PAH compounds	Number of rings	Molecular formula and molecular weight (MW)	Winter		Spring	
			Conc. ( $\text{ng m}^{-3}$ )	% of total	Conc. ( $\text{ng m}^{-3}$ )	% of total
NaP	2-rings	$\text{C}_{10}\text{H}_8$ ,128	10.12	7.22	2.60	6.28
Acy		$\text{C}_{12}\text{H}_8$ ,152	0.16	0.12	0.08	0.20
Ace		$\text{C}_{12}\text{H}_{10}$ ,154	0.15	0.11	0.34	0.83
Flu	3-rings	$\text{C}_{13}\text{H}_{10}$ ,166	1.19	0.85	1.70	4.11
Phe		$\text{C}_{14}\text{H}_{10}$ ,178	3.54	2.52	3.24	7.83
Ant		$\text{C}_{14}\text{H}_{10}$ ,178	0.46	0.33	0.54	1.31
Flua		$\text{C}_{16}\text{H}_{10}$ ,202	8.05	5.74	2.57	6.21
Pyr		$\text{C}_{16}\text{H}_{10}$ ,202	8.93	6.37	2.43	5.87
BaA	4-rings	$\text{C}_{18}\text{H}_{12}$ , 228	11.6	8.27	1.88	4.53
Chr		$\text{C}_{18}\text{H}_{12}$ , 228	15.41	11.0	4.32	10.43
BbF+BjF		$\text{C}_{20}\text{H}_{12}$ , 252	12.19	8.69	3.89	9.39
BkF		$\text{C}_{20}\text{H}_{12}$ , 252	5.58	3.98	1.87	4.50
BaP	5-rings	$\text{C}_{20}\text{H}_{12}$ , 252	10.33	7.37	3.43	8.29
BeP		$\text{C}_{20}\text{H}_{12}$ , 252	12.08	8.61	2.42	5.83
DBA		$\text{C}_{22}\text{H}_{14}$ , 278	2.53	1.8	0.42	1.02
InP	6-rings	$\text{C}_{22}\text{H}_{12}$ , 276	20.74	14.8	5.23	12.62
BghiP		$\text{C}_{22}\text{H}_{12}$ , 276	17.18	12.3	4.46	10.76
LMW-PAHs	2-3 rings		15.62	11.1	8.50	20.6
MMW-PAHs	4-rings		43.99	31.4	11.20	27.0
HMW-PAHs	5-6 rings		80.63	57.5	21.72	52.4
$\Sigma$ PAHs			140.25	100.0	41.42	100.0

1058

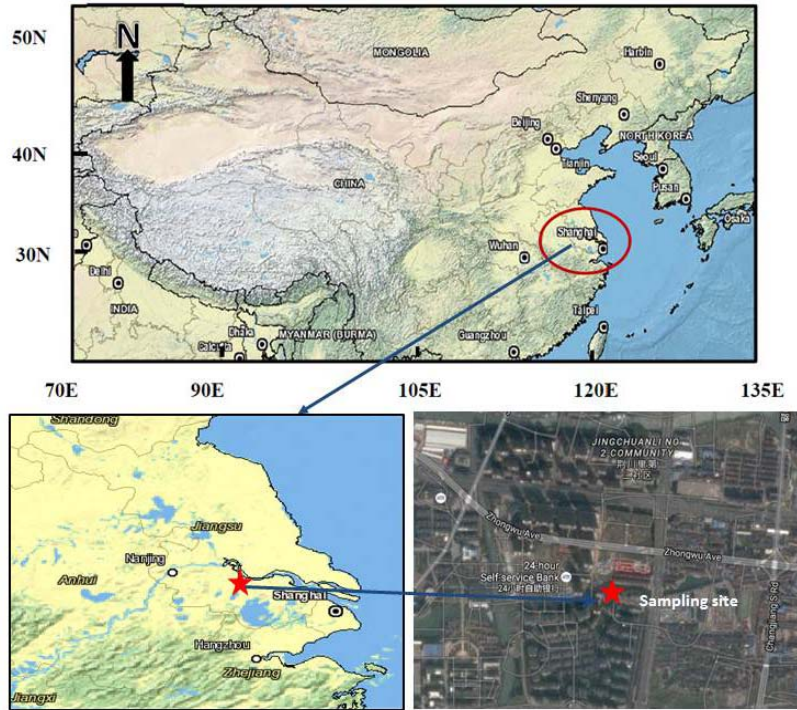
1059 Table 5. Cross-correlation coefficients ( $r$ ) of the measured concentrations of the PAH species  
 1060 and ratios of the mean concentrations between these species from GC-MS (bold) and SP-AMS  
 1061 (italic).

PAHs	C <sub>16</sub> H <sub>10</sub>	C <sub>18</sub> H <sub>12</sub>	C <sub>20</sub> H <sub>12</sub>	C <sub>22</sub> H <sub>12</sub>	Ratio (GC)	Ratio (SP-AMS)
C <sub>16</sub> H <sub>10</sub>	1	-0.250	-0.062	-0.140	<b>C<sub>16</sub>H<sub>10</sub>/C<sub>16</sub>H<sub>10</sub>=1</b>	<i>C<sub>16</sub>H<sub>10</sub><sup>+</sup>/C<sub>16</sub>H<sub>10</sub><sup>+</sup>=1</i>
C <sub>18</sub> H <sub>12</sub>	<b>0.952</b>	<b>1</b>	0.572	0.528	<b>C<sub>16</sub>H<sub>10</sub>/C<sub>18</sub>H<sub>12</sub>=0.84</b>	<i>C<sub>16</sub>H<sub>10</sub><sup>+</sup>/C<sub>18</sub>H<sub>12</sub><sup>+</sup>=0.43</i>
C <sub>20</sub> H <sub>12</sub>	<b>0.936</b>	<b>0.994</b>	1	0.771	<b>C<sub>16</sub>H<sub>10</sub>/C<sub>20</sub>H<sub>12</sub>=0.36</b>	<i>C<sub>16</sub>H<sub>10</sub><sup>+</sup>/C<sub>20</sub>H<sub>12</sub><sup>+</sup>=0.56</i>
C <sub>22</sub> H <sub>12</sub>	<b>0.925</b>	<b>0.986</b>	<b>0.993</b>	1	<b>C<sub>16</sub>H<sub>10</sub>/C<sub>22</sub>H<sub>12</sub>=0.35</b>	<i>C<sub>16</sub>H<sub>10</sub><sup>+</sup>/C<sub>22</sub>H<sub>12</sub><sup>+</sup>=1.17</i>

1062 C<sub>16</sub>H<sub>10</sub>: Flua+Pyr; C<sub>18</sub>H<sub>12</sub>: BaA+Chr; C<sub>20</sub>H<sub>12</sub>: BbF+BjF+BkF+BaP+BeP;

1063 C<sub>22</sub>H<sub>12</sub>: BghiP+InP+DBA

1064



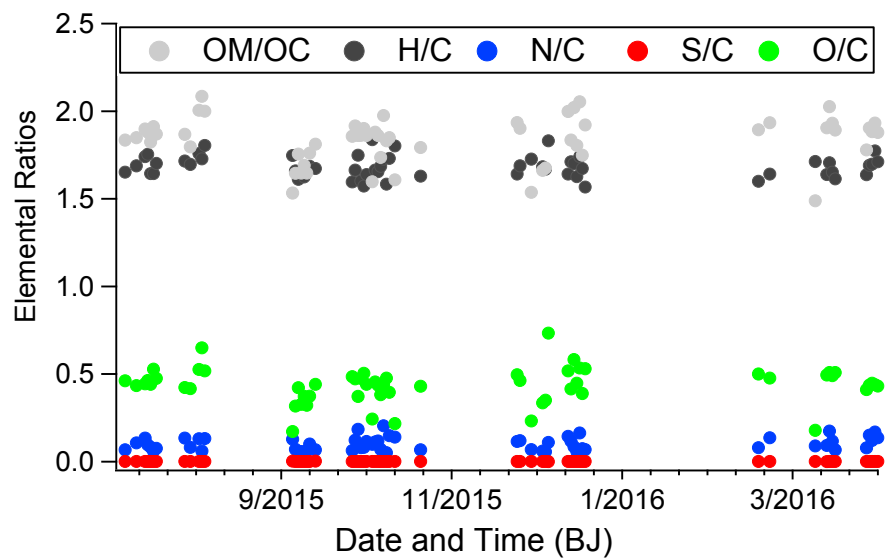
1065

1066 Figure 1. Schematic map of the sampling site and its surroundings.

1067

1068





1069

1070 Figure 2. The atomic elemental ratios for the water-soluble organic aerosols (WSOA)

1071 determined by the SP-AMS.

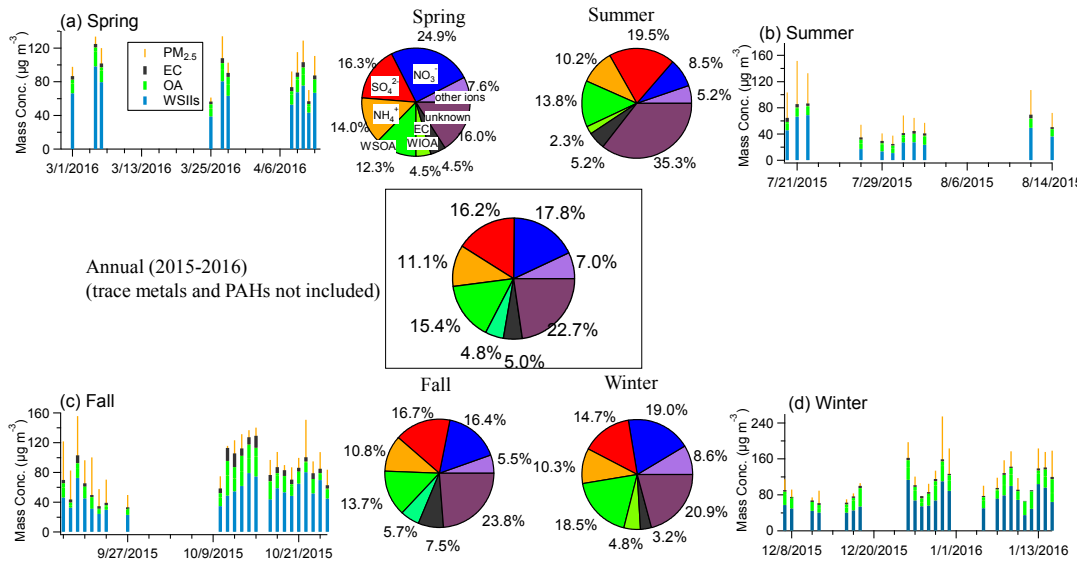
1072

1073

1074

1075

1076



1077

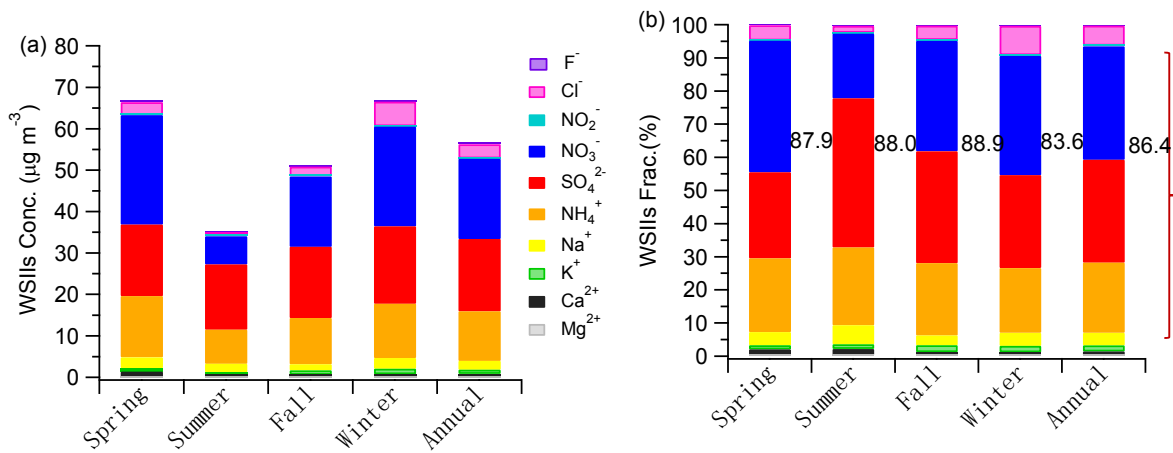
1078 Figure 3. Reconstructed mass (= OA + EC + WSIs) vs. PM<sub>2.5</sub> mass from gravimetric

1079 measurement in (a) spring, (b) summer, (c) fall, (d) winter, and annual. Corresponding pie charts

1080 show the mass percentages of different species to the PM<sub>2.5</sub> mass (trace elements and PAHs are

1081 not included due to sample limitations).

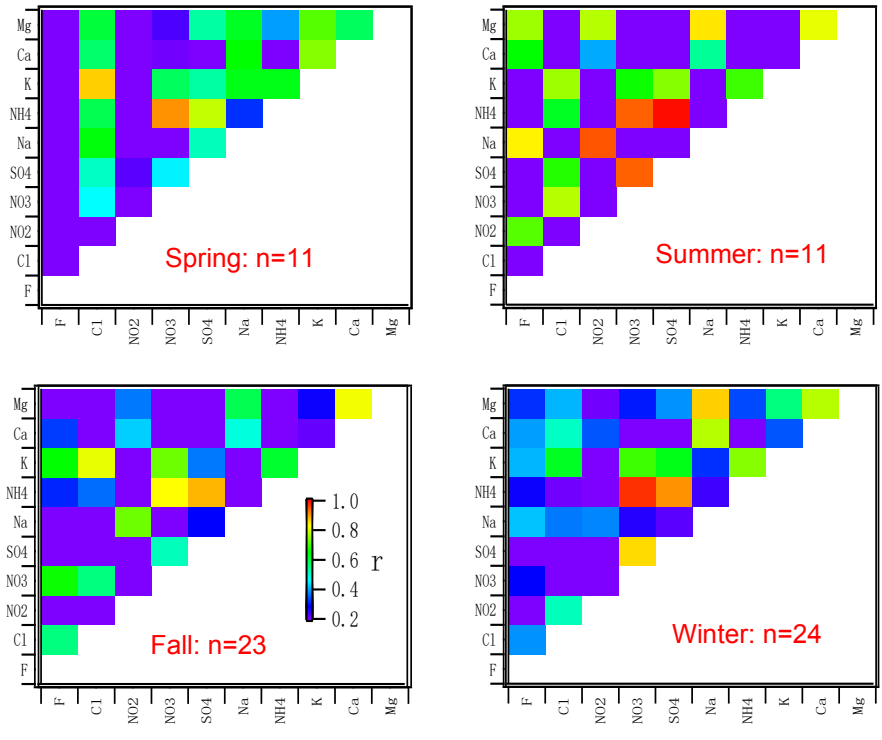
1082



1083

1084

1085 Figure 4. (a) Seasonal variations of average mass concentrations and (b) mass fractional  
 1086 contributions of WSIs in PM<sub>2.5</sub> in Changzhou during 2015-2016. The values marked in (b) are  
 1087 the fractions of three most abundant ions ( $\text{NO}_3^- + \text{SO}_4^{2-} + \text{NH}_4^+$ ) to the total WSIs.  
 1088

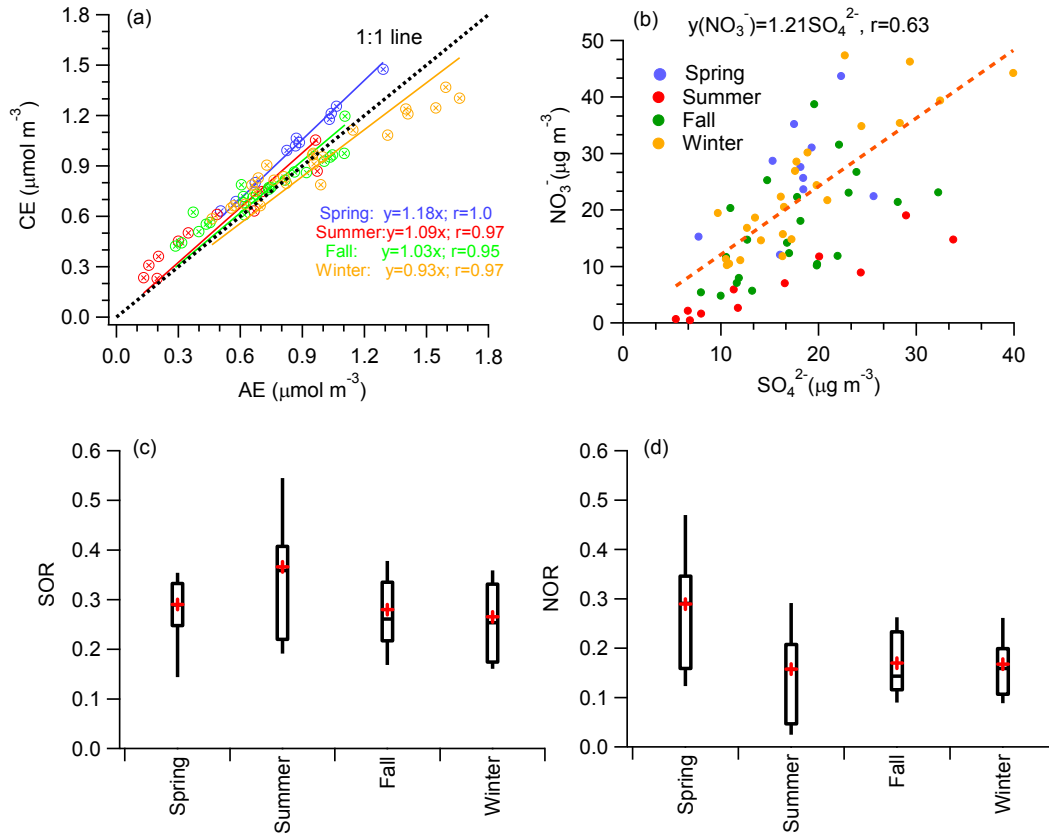


1089

1090 Figure 5. Image plots showing the cross correlation coefficients ( $r$ ) between water-soluble ions

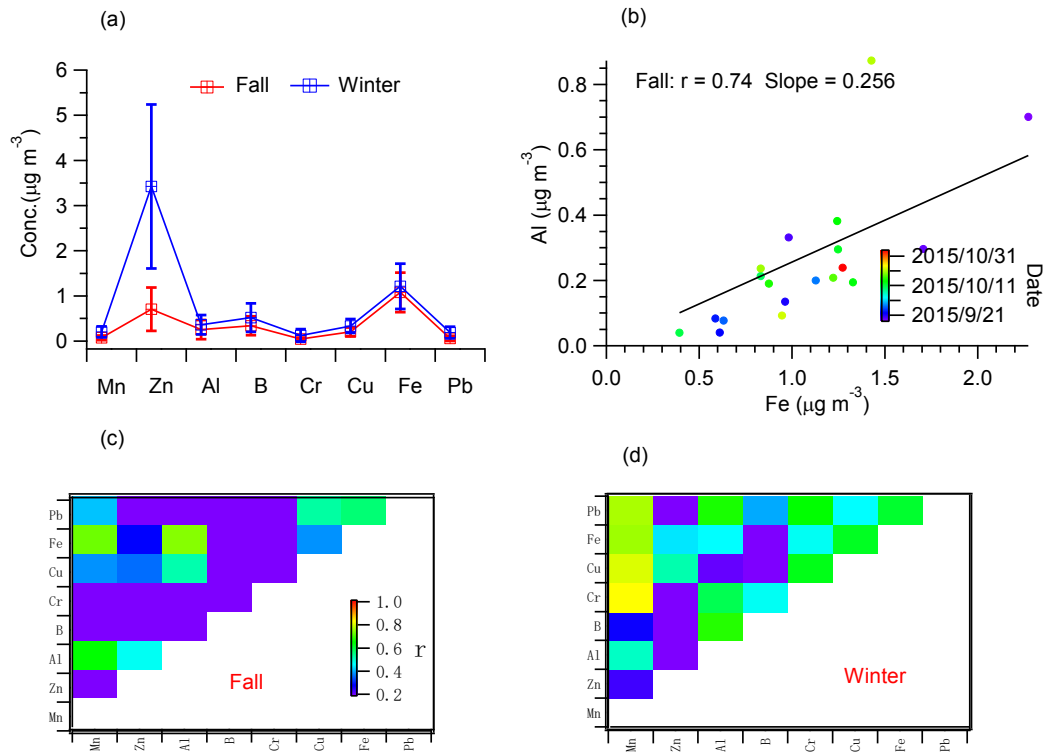
1091 in  $PM_{2.5}$  in four seasons (colored by  $r$ ).

1092



1093  
1094

1095 Figure 6. (a) Scatter plots of molar concentrations of cations vs. anions, (b) scatter plots of  $\text{NO}_3^-$   
 1096 vs.  $\text{SO}_4^{2-}$  concentrations, (c-d) SOR and NOR value during four seasons. In (a), the dashed line  
 1097 refers to 1:1 line. In (b), the dashed line was the averaged fitted line, representing  $\text{NO}_3^-/\text{SO}_4^{2-}$   
 1098 ratio during the entire period. Data in different seasons are shown by different colors for  
 1099 comparison. Linear regression equations were also presented. In (c-d), the crosses represent the  
 1100 mean, the middle bars represent the median, the top and bottom of the box represents the 75<sup>th</sup>  
 1101 and 25<sup>th</sup> percentile, respectively, and the top and bottom whiskers represent the 90<sup>th</sup> and 10<sup>th</sup>  
 1102 percentile, respectively.



1103

1104 Figure 7. (a) Mean mass concentrations of trace elements determined for fall and winter (error

1105 bar represents the measurement uncertainty), (b) scatter plots of Al vs. Fe in fall, and (c-d)

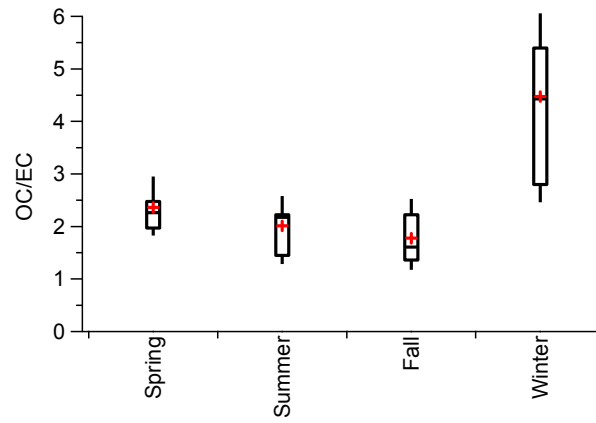
1106 cross-correlation coefficients ( $r$ ) among different trace elements in fall and winter, respectively

1107 (colored by  $r$ ).

1108

1109

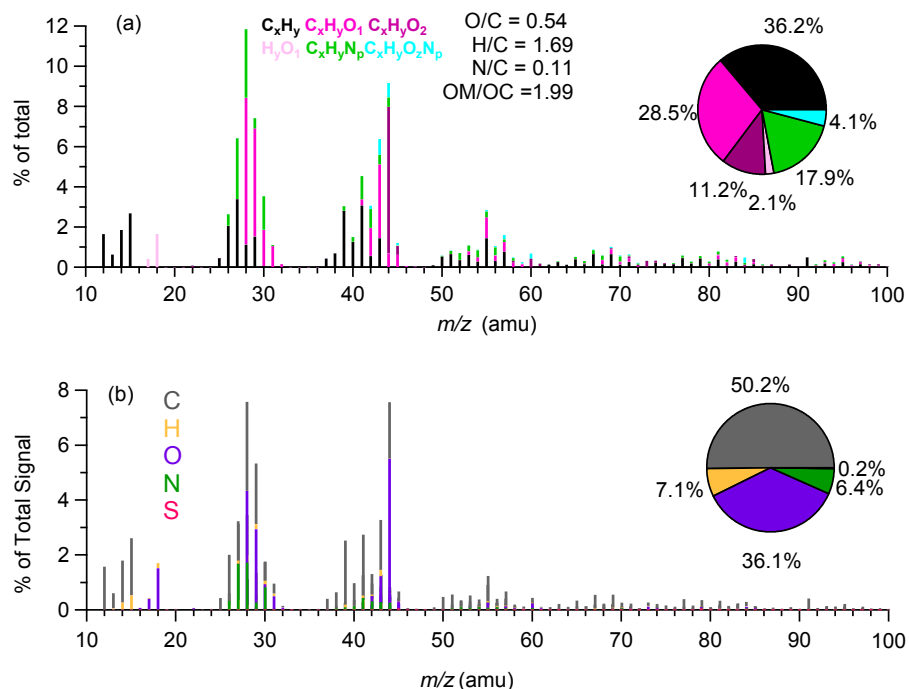
1110



1111

1112 Figure 8. Average OC/EC ratios measured in four seasons (symbols of the box plots are the  
1113 same as described in Figure 6.)

1114



1115

1116 Figure 9. (a) High-resolution mass spectral profile of the WSOA measured by the SP-AMS

1117 (Mass spectrum is classified and colored by six ion families; pie chart shows the mass

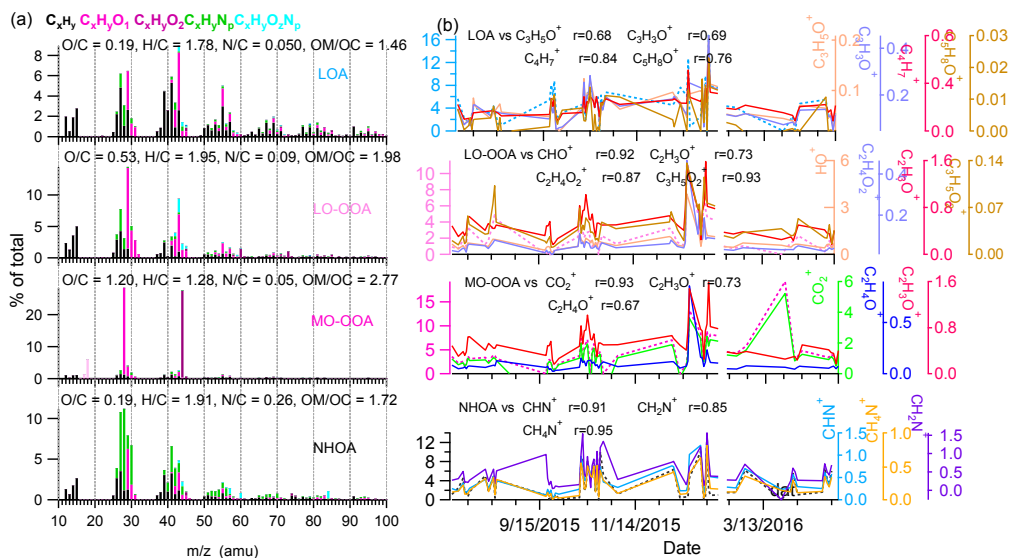
1118 contributions of each ion family to the total MS), (b) Average mass spectrum classified by five

1119 elements (C, H, O, N, and S) (inset pie chart shows mass contributions of the five elements,

1120 respectively).

1121





1122

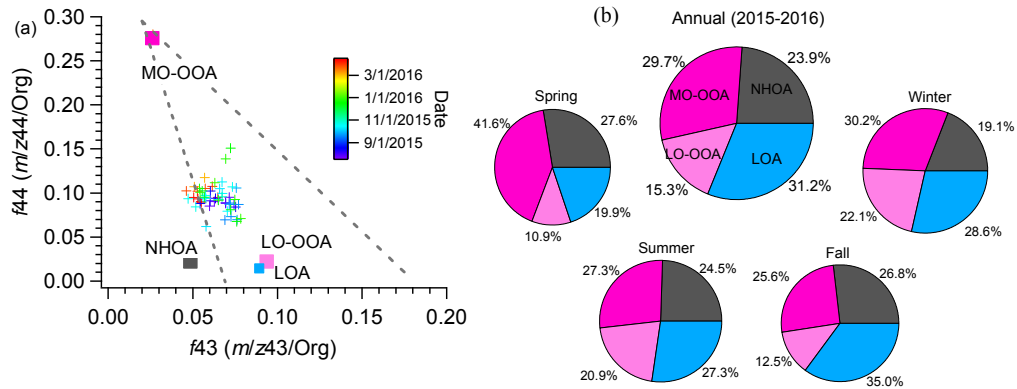
1123 Figure 10. (a) High-resolution mass spectra of nitrogen-enriched hydrocarbon-like OA (NHOA),

1124 local primary OA (LOA), less-oxidized OA (LO-OOA) and more-oxidized OA (MO-OOA)

1125 separated by the PMF analyses, colored by six ion categories, (b) time series of the four WSOA

1126 factors, and corresponding tracer ions.

1127



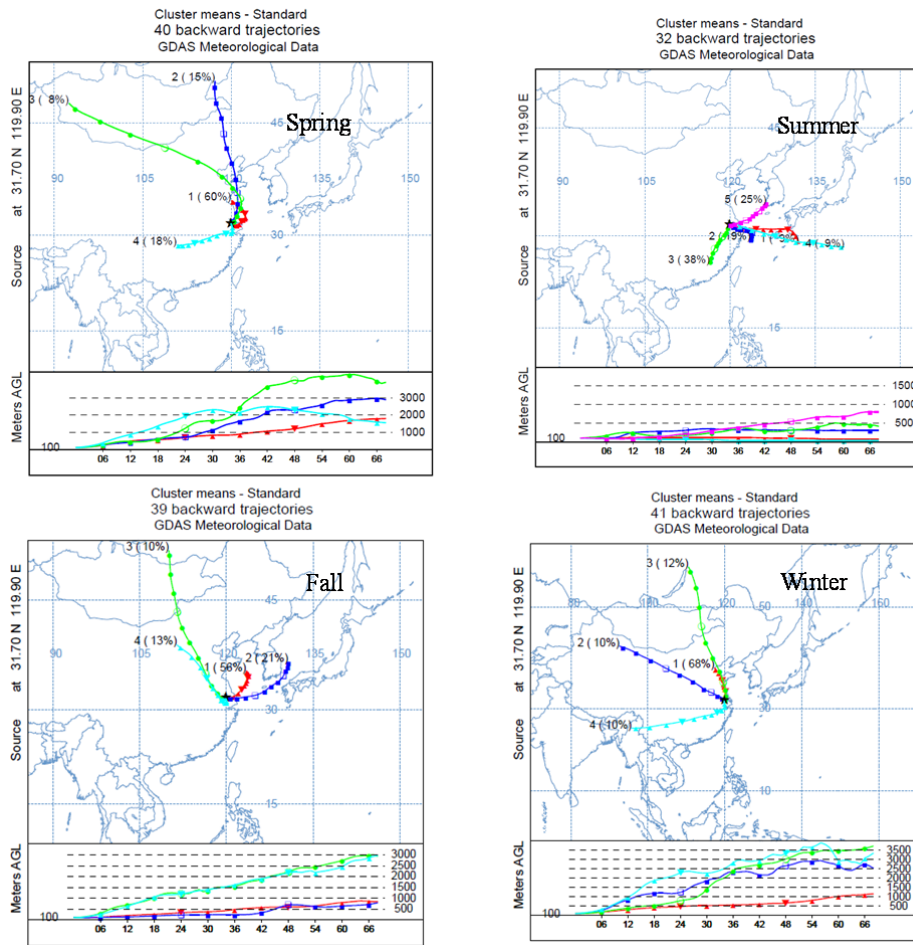
1128

1129 Figure 11. (a) Triangle plot of  $f_{44}$  vs.  $f_{43}$  for all WSOA, and the four WSOA factors identified

1130 by the PMF analyses, (b) pie charts of the mass contributions of four WSOA factors to the total

1131 WSOA in four seasons and the whole sampling period.

1132



1133

1134 Figure 12. Air mass back trajectories across four seasons during the sampling period.

1135